

Nuclear Chemical and Mechanical Instability and the Liquid-Gas Phase Transition in Nuclei

S.J. Lee^{1,2} and A.Z. Mekjian¹

¹*Department of Physics and Astronomy, Rutgers University, Piscataway, NJ 08854 and*

²*Department of Physics, Kyung Hee University, Yongin, KyungGiDo, Korea*

The thermodynamic properties of nuclei are studied in a mean field model using a Skyrme interaction. Properties of two component systems are investigated over the complete range of proton fraction from a system of pure neutrons to a system of only protons. Besides volume, symmetry, and Coulomb effects we also include momentum or velocity dependent forces. Applications of the results developed are then given which include nuclear mechanical and chemical instability and an associated liquid/gas phase transition in two component systems. The velocity dependence leads to further changes in the coexistence curve and nuclear mechanical and chemical instability curves.

I. INTRODUCTION

One primary goal of medium energy nuclear collisions is a detailed study of the thermodynamic properties of strongly interacting nuclear matter [1, 2]. An important feature of these properties is the existence of liquid-gas phase transition. Properties of the nuclear force (long range attraction and short range repulsion) parallel those of a van der Waals system [3] which qualitatively describes a liquid-gas phase transition in atomic systems. The liquid-gas phase transition in nuclei is the first phase transition seen in a strongly interacting system. Relativistic heavy ion collisions are being used to explore a second phase transition from hadronic matter made of mesons and baryons to a quark-gluon phase. Important differences exist between the nuclear interaction and interaction between atoms. Because nuclei are made of neutrons and protons, the phase transition is in a two component or binary system where symmetry energy effects and Coulomb effects play an important role. Moreover, the nuclear force has a velocity dependence. The presence of symmetry energy and a Coulomb interaction effects and also a velocity dependence in the nuclear interaction makes the nuclear case a unique and interesting binary system within the general scope of such systems. Examples of other two component systems are binary alloys and liquid ^3He . For ^3He the two components are spin-up and spin down fluids. The phase structure in such two component systems has some important features. In nuclear systems, isospin fractionation [1, 2, 4, 5, 6, 7] is an example where the monomer gas phase has a large neutron to proton ratio. Ref.[7] is the most recent reference to isospin fractionation and contains further references to it. Both the symmetry energy and Coulomb energy play an important role in this phenomena of isospin fractionation. Nucleons carry spin but very little research has been done in understanding the role of spin in the liquid gas phase structure. However, the crust of neutron stars has features associated with a superfluid phase.

An early study of the nuclear liquid-gas phase transition [3] treated the system as a one component system of nucleons. This study was then extended to two components using a Skyrme interaction [8]. A relativistic mean field model was also developed in Ref.[9] where the role of the symmetry energy was studied in detail. The addition of the Coulomb energy [10, 11] resulted in asymmetries which changed the mechanical and chemical instability regions and binodal surface in pressure P , temperature T and proton fraction y associated with phase coexistence. For one component systems a phase diagram is the more familiar binodal curve of pressure versus density or volume determined by a Maxwell construction. Some other studies of one and two component phase transitions can be found in Refs.[12, 13, 14, 15, 16, 17, 18, 19, 20, 21]. The present work is an extension of our research reported in Refs.[10, 11]. An extended Skyrme interaction is now used in our present study and, for example, includes effects associated with a velocity dependence in the nuclear interaction. Here we will use a simplified form of the velocity dependence. In particular we will use an effective mass approximation for it which includes a density dependent behavior. Our primary goal is to see what qualitative effects a momentum dependence has when superimposed upon an interaction model that does not include them. A momentum dependence study was also given in Ref.[22] using a more refined dependence for it. Our results differ from that of Ref.[22] since we also include Coulomb and surface effects. Coulomb effects lead to an asymmetric behavior in proton fraction [10, 11] of various quantities. In the absence of Coulomb forces a symmetry exists around proton fraction $y = 1/2$. The velocity dependent force modifies nuclear saturation properties and the symmetry energy. Some recent extended studies of symmetry energy can be found in Refs.[23, 24]. The results given below show modifications in chemical and mechanical instability curves arising from an inclusion of a density dependent effective mass. The velocity dependence has a larger effect on the proton rich instability and coexistence features compared to the neutron rich curves. A detailed discussion is given below in Section III and in associated figures. The study of two component nuclear systems with arbitrary neutron/proton ratios will be useful for future RIB (Rare Isotope Beam Facility) experiments and in astrophysical studies such as in neutron stars.

Our paper is divided as follows. The next section discusses the thermodynamic properties of nuclei. It is divided

into two subsections. General results based on a mean field approach are presented in IIA. Specific results based on a Skyrme force for the potential terms, and low and high temperature kinetic energy behavior appear in IIB. This subsection also contains the effects of a velocity dependent interaction and related effective mass results. Then in Sect.III we apply the results of subsection IIA and IIB to the specific issues of: A) mechanical and chemical instability of nuclei and B) the liquid-gas coexistence curve. Results are presented in 9 figures which are discussed. Finally, in Sect.IV a summary and conclusions are given.

II. THERMODYNAMIC PROPERTIES OF NUCLEI IN A MEAN FIELD DESCRIPTION

A. General Results

In this section we present results for the thermodynamic properties of nuclear matter which are extended from the results of Ref.[10] to include a velocity or momentum dependent interaction. The matter is a two component system of protons and neutrons in equilibrium at some temperature T . We first develop expressions for the total energy E as a function of the density ρ_q of each component q and temperature T . The behavior of the energy functional with ρ_q and T can be used to obtain the behavior of the pressure P and chemical potential μ_q for each component of type q . These quantities will also be functions of ρ_q and T . They can then be used to study, for example, a phase transition in the nuclear system.

To begin, we use the fact that at a given temperature $T = 1/\beta$, the proton and neutron constituents are distributed in phase space according to the Wigner function f as

$$f(\vec{r}, \vec{p}) = \sum_q f_q(\vec{r}, \vec{p}), \quad f_q(\vec{r}, \vec{p}) = \frac{\gamma}{h^3} \tilde{f}_q(\vec{r}, \vec{p}) = \frac{\gamma}{h^3} \frac{1}{e^{\beta(\epsilon_q - \mu_q)} + 1} \quad (1)$$

The spin degeneracy factor $\gamma = 2$ and ϵ_q and μ_q are the single particle energy and the chemical potential of particle of type q . Then the particle density ρ and nucleon number A are given by the following equations:

$$\rho(\vec{r}) = \sum_q \rho_q(\vec{r}), \quad \rho_q(\vec{r}) = \int d^3p f_q(\vec{r}, \vec{p}), \quad (2)$$

$$A = \sum_q N_q = \int d^3r \rho(\vec{r}), \quad N_q = \int d^3r \rho_q(\vec{r}) = \int d^3r \int d^3p f_q(\vec{r}, \vec{p}) \quad (3)$$

Defining $\tau(\vec{r})$ as

$$\tau(\vec{r}) = \sum_q \tau_q(\vec{r}), \quad \tau_q(\vec{r}) = \int d^3p \frac{p^2}{h^2} f_q(\vec{r}, \vec{p}) \quad (4)$$

the total energy E is given by

$$E = \int d^3r \mathcal{E}(\vec{r}) = \int d^3r \int d^3p \frac{p^2}{2m} f(\vec{r}, \vec{p}) + \int d^3r \int d^3p U(\vec{r}, \vec{p}) = \int d^3r [\mathcal{E}_K(\vec{r}) + U(\vec{r})] \quad (5)$$

The potential energy density is $U(\vec{r})$, while the $\mathcal{E}_K(\vec{r}) = \frac{\hbar^2}{2m} \tau(\vec{r})$ is the kinetic energy density. The single particle energy ϵ_q is given by

$$\epsilon_q = \frac{\delta E}{\delta f_q} = \frac{\delta \mathcal{E}(\vec{r})}{\delta f_q(\vec{r}, \vec{p})} = \frac{p^2}{2m} + \frac{\delta U}{\delta f_q} = \frac{p^2}{2m} + u_q(\vec{r}, \vec{p}) \quad (6)$$

The $u_q = \frac{\delta U}{\delta f_q}$ is the single particle potential of particle q which may in general be momentum dependent. The chemical potential μ_q is given by ϵ_q at an effective Fermi momentum $p = p_{Fq}$ defined by the following equation:

$$\mu_q = \epsilon_q|_{p=p_{Fq}} = \frac{p_{Fq}^2}{2m} + u_q(\vec{r}, \vec{p}_{Fq}) \quad (7)$$

In order to study a phase transition we need information about the behavior of the pressure when the system is in equilibrium. The general expression for the pressure can be defined dynamically from the total momentum conservation law, $\frac{d}{dt} [\int d^3r \int d^3p \vec{p} f] = - \int d^3r \vec{\nabla}_r \cdot \vec{\Pi} = 0$, using the Vlasov equation as developed in Ref.[21]:

$$\frac{\partial f_q}{\partial t} + (\vec{\nabla}_p \epsilon_q) \cdot (\vec{\nabla}_r f_q) - (\vec{\nabla}_r \epsilon_q) \cdot (\vec{\nabla}_p f_q) = 0 \quad (8)$$

A more general expression is obtained from the hydrodynamic consideration of TDHF in phase space as given in Ref.[26] which reads;

$$\begin{aligned}\vec{\nabla}_r \cdot \overleftrightarrow{\Pi} &= -\frac{d}{dt} \left[\int d^3 p \vec{p} \sum_q f_q(\vec{r}, \vec{p}) \right] = -\sum_q \int d^3 p \vec{p} \left(\frac{\partial f_q}{\partial t} \right) \\ &= \sum_q \int d^3 p \vec{p} \cdot \vec{\nabla}_r \cdot [(\vec{\nabla}_p \epsilon_q) f_q] + \sum_q \int d^3 p \vec{p} \cdot (\vec{\nabla}_r \epsilon_q) f_q\end{aligned}\quad (9)$$

where $\hat{p} = \vec{p}/p$ is a unit vector in the direction of \vec{p} . Using $(\vec{\nabla}_r \epsilon_q) f_q = \vec{\nabla}_r (\epsilon_q f_q) - \epsilon_q \vec{\nabla}_r f_q = \vec{\nabla}_r (\epsilon_q f_q) - \vec{\nabla}_r \mathcal{E}$, the dynamical pressure tensor Π_{ij} is given by

$$\begin{aligned}\Pi_{ij} &= \sum_q \int d^3 p p p_i (\nabla_p^j \epsilon_q) f_q + \delta_{ij} \left[\int d^3 p \sum_q \epsilon_q f_q - \mathcal{E} \right] \\ &= \sum_q \int d^3 p p p_i \nabla_p^j \left(\frac{\delta \mathcal{E}}{\delta f_q} \right) f_q + \delta_{ij} \left[\sum_q \int d^3 p \left(\frac{\delta \mathcal{E}}{\delta f_q} \right) f_q - \mathcal{E} \right] \\ &= \sum_q \int d^3 p p p_i \left[\frac{p_j}{m} + \nabla_p^j \left(\frac{\delta U}{\delta f_q} \right) \right] f_q + \delta_{ij} \left[\sum_q \int d^3 p \left(\frac{\delta U}{\delta f_q} \right) f_q - U \right]\end{aligned}\quad (10)$$

Our previous study [10] focused on a momentum independent potential which gave the following simpler results for the pressure tensor:

$$\Pi_{ij} = \sum_q \int d^3 p \frac{p_i p_j}{m} f_q + \delta_{ij} \left[\sum_q \left(\frac{\delta U}{\delta \rho_q} \right) \rho_q - U \right] = \int d^3 p \sum_q \frac{p_i p_j}{m} f_q + \delta_{ij} \sum_q \rho \rho_q \frac{\delta(U/\rho)}{\delta \rho_q}\quad (11)$$

The diagonal element of Π_{ij} is the pressure $P = \Pi_{ij}$ which simplifies to

$$P = \Pi_{ii} = \sum_q \int d^3 p \frac{p_i^2}{m} f_q + \sum_q \frac{\delta U}{\delta \rho_q} \rho_q - U = P_K + \sum_q u_q \rho_q - U = P_K + P_P\quad (12)$$

The $P_K = \int d^3 p \frac{p_i^2}{m} f = \frac{2}{3} \mathcal{E}_K$ is the kinetic part of the pressure P , while the interaction potential part is $P_P = \sum_q u_q \rho_q - U = \rho^2 \frac{\delta(U/\rho)}{\delta \rho}$. At temperature $T = 0$ the pressure P is related to the derivative of the energy per particle E/A with particle number fixed as

$$P = \Pi_{ii} = -\frac{d(E/A)}{dV} = \rho^2 \frac{d(\mathcal{E}/\rho)}{d\rho}\quad (13)$$

This result applies to a single component system. Below we will give results at non zero temperature for a multi component system. We first proceed with a discussion of the role of the momentum dependence and effective mass.

As mentioned, our study is based on a qualitative study of the role of a momentum dependent interaction and we therefore use a simplifying approximation. Specifically, we use an effective mass with a density dependence and this approximation greatly simplifies our analysis in two component asymmetric and finite nuclear systems. We still include both Coulomb and surface effects since realistic nuclear systems have such terms which are important in their description and stability properties. More refined studies will be developed in future work. When the momentum dependent part is of the form $A(\rho_p, \rho_n) \frac{p^2}{\hbar^2} f$, then it can be incorporated into the Hamiltonian as an effective mass term. In Ref.[22], the momentum dependence is obtained from

$$\int \int d^3 p d^3 p' \frac{f_\tau(\vec{r}, \vec{p}) f'_\tau(\vec{r}, \vec{p}')}{1 + (\vec{p} - \vec{p}')^2 / \Lambda^2}\quad (14)$$

We use an effective mass m_q^*/m approach [25] for Eq.(14) which can further be approximated by expanding the factor $1/(1 + (\vec{p} - \vec{p}')^2 / \Lambda^2)$ to first order in $1 - (\vec{p} - \vec{p}')^2 / \Lambda^2$. Specifically, we write the effective mass behavior of m/m_q^* as

$$\frac{m}{m_q^*} = 1 + A_q(\rho) \frac{2m}{\hbar^2} \quad A_q(\rho) \tau_q(\vec{r}) = \frac{\hbar^2}{2m_q^*} \tau_q(\vec{r}) - \frac{\hbar^2}{2m} \tau_q(\vec{r})\quad (15)$$

Moreover, we have $U(\vec{r}) = U(\rho) + A(\rho)\tau(\vec{r}) = U(\rho) + \sum_q A_q(\rho)\tau_q(\vec{r})$ with $\tau_q(\vec{r})$ of Eq.(4). A momentum dependent single particle potential $u_q(\vec{r}, \vec{p})$ is given by

$$u_q(\vec{r}, \vec{p}) = \frac{\delta U(\vec{r})}{\delta f_q(\vec{r}, \vec{p})} = \frac{\delta U(\rho)}{\delta \rho_q} + \frac{\delta A(\rho)\tau(\vec{r})}{\delta \rho_q} + A_q(\rho)\frac{p^2}{\hbar^2} = \frac{\delta U(\vec{r})}{\delta \rho_q} + A_q(\rho)\frac{p^2}{\hbar^2} \quad (16)$$

The μ_q is related to $u_q(\vec{r}, \vec{p})$ through the result

$$\begin{aligned} \mu_q &= \frac{p_{Fq}^2}{2m} + u_q(\vec{r}, \vec{p}_{Fq}) = \left(1 + A_q(\rho)\frac{2m}{\hbar^2}\right)\frac{p_{Fq}^2}{2m} + \frac{\delta U(\rho)}{\delta \rho_q} + \frac{\delta A(\rho)\tau(\vec{r})}{\delta \rho_q} \\ &= \left(1 + A_q(\rho)\frac{2m}{\hbar^2}\right)\frac{p_{Fq}^2}{2m} + \frac{\delta U(\vec{r})}{\delta \rho_q} = \frac{p_{Fq}^2}{2m_q^*} + \frac{\delta U(\vec{r})}{\delta \rho_q} \end{aligned} \quad (17)$$

Also

$$\vec{\nabla}_p u_q(\vec{r}, \vec{p}) = \vec{\nabla}_p \left(\frac{\delta U(\vec{r})}{\delta f_q} \right) = A_q(\rho)\frac{2\vec{p}}{\hbar^2} \quad (18)$$

and

$$\begin{aligned} \int d^3p u_q f_q &= \int d^3p \left(\frac{\delta U(\vec{r})}{\delta f_q} \right) f_q(\vec{r}, \vec{p}) = \frac{\delta U(\rho)}{\delta \rho_q} \rho_q(\vec{r}) + \frac{\delta A(\rho)\tau(\vec{r})}{\delta \rho_q} \rho_q(\vec{r}) + A_q(\rho)\tau_q(\vec{r}) \\ &= \frac{\delta U(\vec{r})}{\delta \rho_q(\vec{r})} \rho_q(\vec{r}) + A_q(\rho)\tau_q(\vec{r}) \end{aligned} \quad (19)$$

Here ρ and τ are treated as independent variables. Then the pressure tensor Π_{ij} is given by

$$\begin{aligned} \Pi_{ij} &= \sum_q \int d^3p \left(1 + A_q(\rho)\frac{2m}{\hbar^2}\right) \frac{p_i p_j}{m} f_q + \delta_{ij} \left[\sum_q \left(\frac{\delta U(\vec{r})}{\delta \rho_q} \right) \rho_q + A(\rho)\tau(\vec{r}) - U(\vec{r}) \right] \\ &= \int d^3p \sum_q \left(1 + A_q(\rho)\frac{2m}{\hbar^2}\right) \frac{p_i p_j}{m} f_q + \delta_{ij} \sum_q \left[\rho(\vec{r})\rho_q(\vec{r})\frac{\delta(U(\rho)/\rho)}{\delta \rho_q} + \rho_q(\vec{r})\frac{\delta A(\rho)\tau(\vec{r})}{\delta \rho_q} \right] \\ &= \int d^3p \sum_q \frac{p_i p_j}{m_q^*} f_q + \delta_{ij} \sum_q \left[\rho(\vec{r})\rho_q(\vec{r})\frac{\delta(U(\vec{r})/\rho)}{\delta \rho_q} + A(\rho)\tau(\vec{r}) \right] \end{aligned} \quad (20)$$

and the pressure P or diagonal element $\Pi_{ii} = P$ is

$$\begin{aligned} P &= \Pi_{ii} = \sum_q \left(1 + A_q(\rho)\frac{2m}{\hbar^2}\right) \int d^3p \frac{p_i^2}{m} f_q + \sum_q \frac{\delta U(\vec{r})}{\delta \rho_q} \rho_q + A(\rho)\tau(\vec{r}) - U(\vec{r}) \\ &= \sum_q \int d^3p \frac{p_i^2}{m_q^*} f_q + \sum_q \frac{\delta U(\vec{r})}{\delta \rho_q} \rho_q - U(\rho) = P_K^* + P_P \end{aligned} \quad (21)$$

The $P_K^* = \sum_q P_{Kq}^*$ with

$$P_{Kq}^* = \left(1 + A_q(\rho)\frac{2m}{\hbar^2}\right) \int d^3p \frac{p_i^2}{m} f_q = \int d^3p \frac{p^2}{3m_q^*} f_q = \frac{2}{3}\mathcal{E}_K^* \quad (22)$$

is the kinetic pressure with an effective mass correction term, and the second equality is for an isotropic momentum distribution. The potential part of the pressure P_P is given by

$$\begin{aligned} P_P &= \sum_q \frac{\delta U(\vec{r})}{\delta \rho_q} \rho_q - U(\rho) = \sum_q \left[\rho \rho_q \frac{\delta(U(\rho)/\rho)}{\delta \rho_q} + \rho_q \frac{\delta A(\rho)\tau(\vec{r})}{\delta \rho_q} \right] = \sum_q \left[\rho \rho_q \frac{\delta(U(\vec{r})/\rho)}{\delta \rho_q} + A_q(\rho)\tau_q(\vec{r}) \right] \\ &= \rho^2 \frac{\delta(U(\rho)/\rho)}{\delta \rho} + \rho \frac{\delta A(\rho)\tau(\vec{r})}{\delta \rho} = \rho^2 \frac{\delta(U(\vec{r})/\rho)}{\delta \rho} + A(\rho)\tau(\vec{r}) = \rho^2 \frac{\delta(U(\vec{r})/\rho)}{\delta \rho} + \mathcal{E}_K^* - \mathcal{E}_K \end{aligned} \quad (23)$$

The $\mathcal{E}_K = \sum_q \frac{\hbar^2}{2m} \tau_q(\vec{r})$ and

$$\mathcal{E}_K^* = \sum_q \frac{\hbar^2}{2m_q^*} \tau_q(\vec{r}) = \sum_q \left(1 + A_q(\rho) \frac{2m}{\hbar^2}\right) \frac{\hbar^2}{2m} \tau_q(\vec{r}). \quad (24)$$

Also in obtaining this result we use the fact that

$$\sum_q \rho_q \frac{\delta U(\rho, \rho_q)}{\delta \rho_q} = \rho \frac{\delta U(\rho, \rho x_q)}{\delta \rho} \quad (25)$$

which can be shown by looking at the derivative of $B(\rho)C(\rho_p)D(\rho_n) = B(\rho)C(\rho x_p)D(\rho x_n)$. Here the variation ρ must be done after replacing ρ_q by ρx_q .

Other thermodynamic variables, such as S , Ω , F , G are given in Ref.[10]. The entropy S follows, from the distribution \tilde{f}_q of Eq.(1),

$$S = \sum_q S_q = \int d^3r \mathcal{S} = \int d^3r \sum_q \mathcal{S}_q \quad (26)$$

and

$$\begin{aligned} \mathcal{S}_q &= -\frac{\gamma}{\hbar^3} \int d^3p \left[\tilde{f}_q \ln \tilde{f}_q + (1 - \tilde{f}_q) \ln(1 - \tilde{f}_q) \right] \\ &= \beta \int d^3p \epsilon_q f_q + \beta \int d^3p \frac{\vec{p} \cdot \vec{\nabla}_p \epsilon_q}{3} f_q - \beta \mu_q \int d^3p f_q \end{aligned} \quad (27)$$

In equilibrium, from Eqs.(10) and (27)

$$\begin{aligned} TS &= \mathcal{E} + P - \sum_q \mu_q \rho_q = \mathcal{E}_K + P_K - \sum_q (\mu_q - u_q) \rho_q \\ &= \mathcal{E}_K + P_K - \sum_q \frac{p_{Fq}^2}{2m} \rho_q, \end{aligned} \quad (28)$$

The last equality of Eq.(28) is the result of using Eq.(7). For momentum dependent potential the entropy is now

$$\begin{aligned} TS &= \mathcal{E} + P - \sum_q \mu_q \rho_q = \mathcal{E}_K^* + P_K^* - \sum_q \left(\mu_q - \frac{\delta U(\vec{r})}{\delta \rho_q} \right) \rho_q \\ &= \mathcal{E}_K^* + P_K^* - \sum_q \left(1 + A_q(\rho) \frac{2m}{\hbar^2} \right) \frac{p_{Fq}^2}{2m} \rho_q = \mathcal{E}_K^* + P_K^* - \sum_q \frac{p_{Fq}^2}{2m_q^*} \rho_q \end{aligned} \quad (29)$$

where use has been made of Eqs.(17) and (21) to obtain this result. General thermodynamic relations also determine the entropy, pressure and chemical potential [10].

B. Thermodynamic Properties of Nuclear Matter based on a Skyrme Interaction

We now use a Skyrme interaction to develop expressions for the potential U . Once the potential energy U in Eq.(5) is known, then questions related to mechanical and chemical instability and the possibility of a phase transition of the system can be studied using Eqs.(1) – (29). The potential energy U determines ϵ_q and μ_q and the potential energy part of E and P . Then for fixed T and N_q , the Wigner function f and p_{Fq} are determined and thus the kinetic terms of E , μ_q , and P . Using these results, the entropy \mathcal{S} can be determined. For a nuclear system of proton (ρ_p) and neutron (ρ_n), this gives the local potential energy density as

$$\begin{aligned} U(\rho_q) &= \frac{t_0}{2} \left(1 + \frac{x_0}{2}\right) \rho^2 - \frac{t_0}{2} \left(\frac{1}{2} + x_0\right) \sum_q \rho_q^2 + \frac{t_3}{12} \left(1 + \frac{x_3}{2}\right) \rho^{\alpha+2} - \frac{t_3}{12} \left(\frac{1}{2} + x_3\right) \rho^\alpha \sum_q \rho_q^2 \\ &+ \frac{1}{4} \left[t_1 \left(1 + \frac{x_1}{2}\right) + t_2 \left(1 + \frac{x_2}{2}\right) \right] \rho \tau - \frac{1}{4} \left[t_1 \left(\frac{1}{2} + x_1\right) - t_2 \left(\frac{1}{2} + x_2\right) \right] \sum_q \rho_q \tau_q \\ &+ C \rho^\beta \rho_p^2 + C_s \rho^\eta \end{aligned} \quad (30)$$

TABLE I: Skyrme parameters used here are in MeV and fm units [11]. For t_1 and t_2 , the SkM parameter values are used.

t_0	x_0	t_3	x_3	α
-1089.0	-1/6	17480.4	-1/2	1
		Momentum-Dep.	Momentum-Indep.	
	t_1	251.11	0	
	x_1	-1/2	-1/2	
	t_2	-150.66	0	
	x_2	-1/2	-1/2	
Effective mass m^*/m		0.895626	1	
Binding energy E_B/A		13.1057	15.54447	
Fermi energy E_F		31.8018	34.2101	
Saturation density ρ_0		0.1283	0.143145	
Symmetry energy S_V		23.4791	24.39379	
Compressibility κ		307.780	361.9045	

Here $C\rho^\beta = \frac{4\pi}{5}e^2R^2$ and $C_s\rho^\eta = \frac{4\pi R^2\sigma(\rho)}{V} = \frac{(4\pi r_0^2\sigma)}{\sqrt{1/3}}\rho^{2/3}$ when we approximate the Coulomb and surface effects as coming from a finite uniform sphere of radius $R = r_0A^{1/3}$ with total charge Z ($U_C = \frac{3}{5}\frac{e^2Z^2}{RV}$) [10]. The values for the force parameters used here are given in Table I. We define an effective mass m_q^* as

$$\frac{m}{m_q^*} = 1 + \frac{2m}{\hbar^2} \left\{ \frac{1}{4} \left[t_1 \left(1 + \frac{x_1}{2} \right) + t_2 \left(1 + \frac{x_2}{2} \right) \right] \rho - \frac{1}{4} \left[t_1 \left(\frac{1}{2} + x_1 \right) - t_2 \left(\frac{1}{2} + x_2 \right) \right] \rho_q \right\} \quad (31)$$

Then the momentum dependent potential term becomes

$$\begin{aligned} A_q(\rho) &= \frac{\hbar^2}{2m_q^*} - \frac{\hbar^2}{2m} = \frac{1}{4} \left[t_1 \left(1 + \frac{x_1}{2} \right) + t_2 \left(1 + \frac{x_2}{2} \right) \right] \rho - \frac{1}{4} \left[t_1 \left(\frac{1}{2} + x_1 \right) - t_2 \left(\frac{1}{2} + x_2 \right) \right] \rho_q \\ &= \frac{\hbar^2}{2m} \left[-1 + 1 + \frac{2m}{\hbar^2} \left\{ \frac{1}{4} \left[t_1 \left(1 + \frac{x_1}{2} \right) + t_2 \left(1 + \frac{x_2}{2} \right) \right] \rho - \frac{1}{4} \left[t_1 \left(\frac{1}{2} + x_1 \right) - t_2 \left(\frac{1}{2} + x_2 \right) \right] \rho_q \right\} \right] \end{aligned} \quad (32)$$

For a symmetric nucleus, $N = Z$, $\rho_q = \rho/2$, and thus

$$U(\rho) = \frac{3}{8}t_0\rho^2 + \frac{3}{48}t_3\rho^{\alpha+2} + \frac{3}{16}(t_1 + t_2)\rho\tau + C\rho^\beta\rho_p^2 + C_s\rho^\eta \quad (33)$$

This potential energy determines the interaction dependent terms of \mathcal{E} , P , ϵ_q , and μ_q which depend on densities without an explicit T dependence.

For a momentum dependent potential energy as in Eq.(30), $\epsilon_q - \mu_q = (p^2 - p_{Fq}^2)/(2m_q^*)$ where the effective mass m_q^* is independent of the momentum independent part of potential and the Wigner function of Eq.(1) becomes

$$\tilde{f}_q(\vec{r}, \vec{p}) = \frac{1}{e^{\beta(\epsilon_q - \mu_q)} + 1} = \frac{1}{e^{\beta(p^2 - p_{Fq}^2)/(2m_q^*)} + 1} \quad (34)$$

Thus we can evaluate the kinetic terms in \mathcal{E} , P , and μ_q which are functions of T and p_{Fq} . Defining the Fermi integral $F_\alpha(\eta)$, with effective mass m_q^* ,

$$F_\alpha(\eta_q) = \int_0^\infty \frac{x^\alpha}{1 + e^{x - \eta_q}} dx = \left(\frac{\lambda_q^2}{4\pi\hbar^2} \right)^{\alpha+1} \int_0^\infty \frac{2p^{2\alpha+1} dp}{1 + e^{\beta p^2/2m_q^* - \eta_q}}, \quad (35)$$

$$\eta_q = \beta \left(\mu_q - \frac{\delta U(\vec{r})}{\delta \rho_q} \right) = \beta p_{Fq}^2/(2m_q^*) = p_{Fq}^2/(2m_q^*T) = \ln z_q, \quad (36)$$

$$\lambda_q = \sqrt{2\pi\hbar^2/m_q^*T} \quad (37)$$

we can write, for $f(\vec{r}, \vec{p}) = f(\vec{r}, p)$,

$$\rho_q = \int d^3p f_q(\vec{r}, \vec{p}) = \frac{\gamma}{h^3} \int d^3p \frac{1}{e^{\beta(p^2 - p_{Fq}^2)/(2m_q^*)} + 1} = \lambda_q^{-3} \frac{2\gamma}{\sqrt{\pi}} F_{1/2}(\eta_q), \quad (38)$$

$$\epsilon_{Fq}^* \equiv \frac{p_{Fq}^2}{2m_q^*} = \frac{\hbar^2}{2m_q^*} \left(\frac{6\pi^2}{\gamma} \rho_q \right)^{2/3} = \frac{m}{m_q^*} \epsilon_{Fq}, \quad \epsilon_{Fq} = \frac{\hbar^2}{2m} \left(\frac{6\pi^2}{\gamma} \rho_q \right)^{2/3}, \quad (39)$$

$$\begin{aligned} \tau_q &= \int d^3p \frac{p^2}{\hbar^2} f_q(\vec{r}, \vec{p}) = \frac{\gamma}{\hbar^3} \int d^3p \frac{p^2}{\hbar^2} \frac{1}{e^{\beta(p^2 - p_{Fq}^2)/(2m_q^*)} + 1} \\ &= 8\gamma\sqrt{\pi}\lambda_q^{-5} F_{3/2}(\eta_q) = \frac{1}{\beta} \frac{2m_q^*}{\hbar^2} \frac{2\gamma}{\sqrt{\pi}} \lambda_q^{-3} F_{3/2}(\eta_q) = \frac{2m}{\hbar^2} \mathcal{E}_{Kq} = \frac{2m_q^*}{\hbar^2} \mathcal{E}_{Kq}^*, \end{aligned} \quad (40)$$

$$\begin{aligned} \mathcal{E}_{Kq} &= \frac{\hbar^2}{2m} \tau_q = \frac{3}{2} P_{Kq} = \int d^3p \frac{p^2}{2m} f_q(\vec{r}, \vec{p}) = \frac{\gamma}{\hbar^3} \int d^3p \frac{p^2}{2m} \frac{1}{e^{\beta(p^2 - p_{Fq}^2)/(2m_q^*)} + 1} \\ &= \frac{4\gamma\hbar^2\sqrt{\pi}}{m} \lambda_q^{-5} F_{3/2}(\eta_q) = \frac{m_q^*}{m} \frac{1}{\beta} \frac{2\gamma}{\sqrt{\pi}} \lambda_q^{-3} F_{3/2}(\eta_q), \end{aligned} \quad (41)$$

$$\begin{aligned} \mathcal{E}_{Kq}^* &= \frac{\hbar^2}{2m_q^*} \tau_q = \frac{3}{2} P_{Kq}^* = \int d^3p \frac{p^2}{2m_q^*} f_q(\vec{r}, \vec{p}) = \frac{\gamma}{\hbar^3} \int d^3p \frac{p^2}{2m_q^*} \frac{1}{e^{\beta(p^2 - p_{Fq}^2)/(2m_q^*)} + 1} \\ &= \frac{4\gamma\hbar^2\sqrt{\pi}}{m_q^*} \lambda_q^{-5} F_{3/2}(\eta_q) = \frac{1}{\beta} \frac{2\gamma}{\sqrt{\pi}} \lambda_q^{-3} F_{3/2}(\eta_q) \end{aligned} \quad (42)$$

Here ϵ_{Fq} is the chemical potential at absolute zero or Fermi energy and p_{Fq} is the effective Fermi momentum at T (which is related to density ρ_q through Eq.(38)). The particle number $N_q = \int d^3r \rho(\vec{r})$ determines the effective Fermi momentum $p_{Fq}(\vec{r})$ or η_q at T , in terms of density $\rho_q(\vec{r})$,

$$\eta_q(\rho_q, T) = \beta \left(\mu_q - \frac{\delta U(\vec{r})}{\delta \rho_q} \right) = \beta \frac{p_{Fq}^2}{2m_q^*} = F_{1/2}^{-1} \left(\frac{\sqrt{\pi}}{2\gamma} \lambda_q^3 \rho_q \right) \quad (43)$$

For multi(two)-component systems with potential energy given by Eq.(30), with a given ρ_q (or p_{Fq}) and T , the thermodynamic properties are as follows. The chemical potential is given by

$$\begin{aligned} \mu_q(\rho_q, T) &= T\eta_q(\rho_q, T) + \frac{\delta U(\vec{r})}{\delta \rho_q} \\ &= T\eta_q(\rho_q, T) + t_0 \left(1 + \frac{x_0}{2} \right) \rho + \frac{t_3}{12} \left(1 + \frac{x_3}{2} \right) (\alpha + 2) \rho^{\alpha+1} - \frac{t_3}{12} \left(\frac{1}{2} + x_3 \right) \alpha \rho^{\alpha+1} \\ &\quad - t_0 \left(\frac{1}{2} + x_0 \right) \rho_q + \frac{t_3}{12} \left(\frac{1}{2} + x_3 \right) (\alpha - 1) 2\rho^\alpha \rho_q - \frac{t_3}{12} \left(\frac{1}{2} + x_3 \right) 2\alpha \rho^{\alpha-1} \rho_q^2 \\ &\quad + \frac{1}{4} \left[t_1 \left(1 + \frac{x_1}{2} \right) + t_2 \left(1 + \frac{x_2}{2} \right) \right] \tau - \frac{1}{4} \left[t_1 \left(\frac{1}{2} + x_1 \right) - t_2 \left(\frac{1}{2} + x_2 \right) \right] \tau_q \\ &\quad + C\beta\rho^{\beta-1} \rho_p^2 + 2C\rho^\beta \rho_p \delta_{q,p} + \eta C_s \rho^{\eta-1}. \end{aligned} \quad (44)$$

The equation of state has a behavior determined by

$$\begin{aligned} P(\rho_q, T) &= \sum_q \frac{2}{3} \mathcal{E}_{Kq}^*(\rho_q, T) + \rho^2 \frac{\delta(U(\rho)/\rho)}{\delta \rho} + \rho \frac{\delta A(\rho)\tau(\vec{r})}{\delta \rho} \\ &= \sum_q \left[\frac{5}{3} \mathcal{E}_{Kq}^*(\rho_q, T) - \mathcal{E}_{Kq}(\rho_q, T) \right] + \rho^2 \frac{\delta(U(\vec{r})/\rho)}{\delta \rho} \\ &= \sum_q \left[\frac{5}{3} \mathcal{E}_{Kq}^*(\rho_q, T) - \mathcal{E}_{Kq}(\rho_q, T) \right] + \frac{t_0}{2} \left(1 + \frac{x_0}{2} \right) \rho^2 + \frac{t_3}{12} \left(1 + \frac{x_3}{2} \right) (\alpha + 1) \rho^{\alpha+2} \\ &\quad - \frac{t_0}{2} \left(\frac{1}{2} + x_0 \right) \sum_q \rho_q^2 - \frac{t_3}{12} \left(\frac{1}{2} + x_3 \right) (\alpha + 1) \rho^\alpha \sum_q \rho_q^2 \\ &\quad + C(\beta + 1) \rho^\beta \rho_p^2 + C_s(\eta - 1) \rho^\eta. \end{aligned} \quad (45)$$

The energy density is

$$\mathcal{E}(\rho_q, T) = \sum_q \mathcal{E}_{Kq}(\rho_q, T) + U(\vec{r}) = \sum_q \mathcal{E}_{Kq}^*(\rho_q, T) + U(\rho)$$

$$\begin{aligned}
&= \sum_q \mathcal{E}_{Kq}^*(\rho_q, T) \\
&\quad + \frac{t_0}{2} \left(1 + \frac{x_0}{2}\right) \rho^2 - \frac{t_0}{2} \left(\frac{1}{2} + x_0\right) \sum_q \rho_q^2 + \frac{t_3}{12} \left(1 + \frac{x_3}{2}\right) \rho^{\alpha+2} - \frac{t_3}{12} \left(\frac{1}{2} + x_3\right) \rho^\alpha \sum_q \rho_q^2 \\
&\quad + C\rho^\beta \rho_p^2 + C_s \rho^\eta
\end{aligned} \tag{46}$$

and the entropy can be obtained from

$$TS(\rho_q, T) = \sum_q \frac{5}{3} \mathcal{E}_{Kq}^*(\rho_q, T) - \sum_q \left(\mu_q - \frac{\delta U(\vec{r})}{\delta \rho_q}\right) \rho_q = \sum_q \frac{5}{3} \mathcal{E}_{Kq}^*(\rho_q, T) - T \sum_q \eta_q(\rho_q, T) \rho_q. \tag{47}$$

Once we evaluate $F_{1/2}(\eta)$ and $F_{3/2}(\eta)$, or more directly $\eta = F_{1/2}^{-1}(\chi)$ and $F_{3/2}(\eta)$, we can evaluate various thermodynamic quantities in terms of ρ_q and T .

For low temperature and high density limit, $\lambda^3 \rho$ large, i.e., when the average de Broglie thermal wavelength λ is larger than the average interparticle separation $\rho^{-1/3}$, we can use a nearly degenerate (Fermi gas) approximations [27] for $F_{1/2}$ to obtain

$$\begin{aligned}
\eta_q(\rho_q, T) &= \beta \left(\mu_q - \frac{\delta U(\vec{r})}{\delta \rho_q}\right) = \beta \frac{p_{Fq}^2}{2m_q^*} = F_{1/2}^{-1} \left(\frac{\sqrt{\pi}}{2\gamma} \lambda_q^3 \rho_q\right) = \beta \epsilon_{Fq}^* \left[1 - \frac{\pi^2}{12} \left(\frac{T}{\epsilon_{Fq}^*}\right)^2 + \dots\right] \\
&= \beta \frac{\hbar^2}{2m_q^*} \left(\frac{6\pi^2}{\gamma}\right)^{2/3} \left[\rho_q^{2/3} - \frac{\pi^2 m_q^{*2}}{3\hbar^4} \left(\frac{\gamma}{6\pi^2}\right)^{4/3} T^2 \rho_q^{-2/3} + \dots\right],
\end{aligned} \tag{48}$$

$$\begin{aligned}
\mathcal{E}_{Kq}^*(\rho_q, T) &= \frac{2\gamma}{\beta\sqrt{\pi}} \lambda_q^{-3} F_{3/2}(\eta_q) = \frac{3}{2} P_{Kq}^* = \frac{3}{5} \rho_q \epsilon_{Fq}^* \left[1 + \frac{5\pi^2}{12} \left(\frac{T}{\epsilon_{Fq}^*}\right)^2 + \dots\right] \\
&= \frac{3\hbar^2}{10m_q^*} \left(\frac{6\pi^2}{\gamma}\right)^{2/3} \left[\rho_q^{5/3} + \frac{5\pi^2 m_q^{*2}}{3\hbar^4} \left(\frac{\gamma}{6\pi^2}\right)^{4/3} T^2 \rho_q^{1/3} + \dots\right],
\end{aligned} \tag{49}$$

$$\begin{aligned}
\tau_q(\rho_q, T) &= \frac{2m_q^*}{\hbar^2} \mathcal{E}_{Kq}^* = \frac{3}{5} \frac{2m_q^*}{\hbar^2} \rho_q \epsilon_{Fq}^* \left[1 + \frac{5\pi^2}{12} \left(\frac{T}{\epsilon_{Fq}^*}\right)^2 + \dots\right] \\
&= \frac{3}{5} \left(\frac{6\pi^2}{\gamma}\right)^{2/3} \rho_q^{5/3} \left[1 + \frac{5\pi^2}{12} \left(\frac{T}{\epsilon_{Fq}^*}\right)^2 + \dots\right] \\
&= \frac{3}{5} \left(\frac{6\pi^2}{\gamma}\right)^{2/3} \left[\rho_q^{5/3} + \frac{5\pi^2 m_q^{*2}}{3\hbar^4} \left(\frac{\gamma}{6\pi^2}\right)^{4/3} T^2 \rho_q^{1/3} + \dots\right]
\end{aligned} \tag{50}$$

In the other limit where $\lambda_q^3 \rho$ is small, we have a nearly non-degenerate Fermi gas (classical ideal gas) and the resulting equations are given by an ideal gas in leading order with higher order corrections [27] as

$$\eta_q(\rho_q, T) = \beta \left(\mu_q - \frac{\delta U(\vec{r})}{\delta \rho_q}\right) = \ln \left[\frac{\rho_q \lambda_q^3}{\gamma} \left(1 + \frac{1}{2\sqrt{2}} \frac{\rho_q \lambda_q^3}{\gamma} + \dots\right)\right] \approx \ln \left(\frac{\rho_q \lambda_q^3}{\gamma}\right) + \frac{1}{2\sqrt{2}} \left(\frac{\rho_q \lambda_q^3}{\gamma}\right), \tag{51}$$

$$\mathcal{E}_{Kq}^*(\rho_q, T) = \frac{3}{2} P_{Kq}^* = \frac{3}{2} \rho_q T \left[1 + \frac{1}{2^{5/2}} \frac{\rho_q \lambda_q^3}{\gamma} + \left(\frac{1}{8} - \frac{2}{3^{5/2}}\right) \left(\frac{\rho_q \lambda_q^3}{\gamma}\right)^2 + \dots\right], \tag{52}$$

$$\tau_q(\rho_q, T) = \frac{2m_q^*}{\hbar^2} \mathcal{E}_{Kq}^* = \frac{2m_q^*}{\hbar^2} \frac{3}{2} \rho_q T \left[1 + \frac{1}{2^{5/2}} \frac{\rho_q \lambda_q^3}{\gamma} + \left(\frac{1}{8} - \frac{2}{3^{5/2}}\right) \left(\frac{\rho_q \lambda_q^3}{\gamma}\right)^2 + \dots\right] \tag{53}$$

For a nuclear system with protons and neutrons with the interaction given by Eq.(30), the non-degenerate Fermi gas limit of Eqs.(51), (52) and (53) leads to the following set of equations. The chemical potential has a behavior

determined by

$$\begin{aligned}
\mu_q(\rho, y, T) = & T \ln \left[\left(\frac{\lambda_q^3}{\gamma} \right) \rho_q \right] + \frac{T}{2\sqrt{2}} \left(\frac{\lambda_q^3}{\gamma} \right) \rho_q \\
& + \frac{1}{4} \left[t_1 \left(1 + \frac{x_1}{2} \right) + t_2 \left(1 + \frac{x_2}{2} \right) \right] \frac{3}{2} T \sum_q \frac{2m_q^*}{\hbar^2} \left[\rho_q + \frac{\lambda_q^3}{2^{5/2}\gamma} \rho_q^2 \right] \\
& - \frac{1}{4} \left[t_1 \left(\frac{1}{2} + x_1 \right) - t_2 \left(\frac{1}{2} + x_2 \right) \right] \frac{3}{2} T \frac{2m_q^*}{\hbar^2} \left[\rho_q + \frac{\lambda_q^3}{2^{5/2}\gamma} \rho_q^2 \right] \\
& + t_0 \left(1 + \frac{x_0}{2} \right) \rho + \frac{t_3}{12} \left(1 + \frac{x_3}{2} \right) (\alpha + 2) \rho^{\alpha+1} - \frac{t_3}{12} \left(\frac{1}{2} + x_3 \right) \alpha \rho^{\alpha+1} \\
& - t_0 \left(\frac{1}{2} + x_0 \right) \rho_q + \frac{t_3}{12} \left(\frac{1}{2} + x_3 \right) (\alpha - 1) 2 \rho^\alpha \rho_q - \frac{t_3}{12} \left(\frac{1}{2} + x_3 \right) 2 \alpha \rho^{\alpha-1} \rho_q^2 \\
& + C \beta \rho^{\beta-1} \rho_p^2 + 2C \rho^\beta \rho_p \delta_{q,p} + \eta C_s \rho^{\eta-1}.
\end{aligned} \tag{54}$$

The equation of state has a form given by

$$\begin{aligned}
P(\rho, y, T) = & \frac{5}{2} T \rho + \frac{5}{2} \frac{T}{2\sqrt{2}} \sum_q \left(\frac{\lambda_q^3}{\gamma} \right) \left(\frac{\rho_q^2}{2} \right) - \frac{3}{2} T \sum_q \frac{m_q^*}{m} \left[\rho_q + \frac{1}{2\sqrt{2}} \left(\frac{\lambda_q^3}{\gamma} \right) \left(\frac{\rho_q^2}{2} \right) \right] \\
& + \frac{t_0}{2} \left(1 + \frac{x_0}{2} \right) \rho^2 + \frac{t_3}{12} \left(1 + \frac{x_3}{2} \right) (\alpha + 1) \rho^{\alpha+2} \\
& - \frac{t_0}{2} \left(\frac{1}{2} + x_0 \right) \sum_q \rho_q^2 - \frac{t_3}{12} \left(\frac{1}{2} + x_3 \right) (\alpha + 1) \rho^\alpha \sum_q \rho_q^2 \\
& + C(\beta + 1) \rho^\beta \rho_p^2 + C_s (\eta - 1) \rho^\eta.
\end{aligned} \tag{55}$$

The energy density is

$$\begin{aligned}
\mathcal{E}(\rho, y, T) = & \frac{3}{2} T \rho + \frac{3}{2} \frac{T}{2\sqrt{2}} \sum_q \left(\frac{\lambda_q^3}{\gamma} \right) \left(\frac{\rho_q^2}{2} \right) \\
& + \frac{t_0}{2} \left(1 + \frac{x_0}{2} \right) \rho^2 - \frac{t_0}{2} \left(\frac{1}{2} + x_0 \right) \sum_q \rho_q^2 + \frac{t_3}{12} \left(1 + \frac{x_3}{2} \right) \rho^{\alpha+2} - \frac{t_3}{12} \left(\frac{1}{2} + x_3 \right) \rho^\alpha \sum_q \rho_q^2 \\
& + C \rho^\beta \rho_p^2 + C_s \rho^\eta
\end{aligned} \tag{56}$$

and the entropy is

$$TS(\rho, y, T) = \frac{5}{2} T \rho - T \sum_q \rho_q \ln \left(\frac{\lambda_q^3}{\gamma} \rho_q \right) + \frac{T}{2\sqrt{2}} \sum_q \left(\frac{\lambda_q^3}{\gamma} \right) \left(\frac{\rho_q^2}{4} \right) \tag{57}$$

The effective mass m_q^* and thus λ_q are, in general, isospin dependent [25]. However we will consider an isospin independent effective mass here for simplicity in this present study. For the case of $m_q^* = m^*$ with $\lambda_q = \lambda$ (such as the case of $x_1 = x_2 = -1/2$), these equations become:

$$\begin{aligned}
\mu_q(\rho, y, T) = & T \ln \left[\left(\frac{\lambda^3}{\gamma} \right) \left(\frac{\rho}{2} \pm (2y - 1) \frac{\rho}{2} \right) \right] + \frac{T}{2\sqrt{2}} \left(\frac{\lambda^3}{\gamma} \right) \left(\frac{\rho}{2} \pm (2y - 1) \frac{\rho}{2} \right) \\
& + \frac{1}{4} \left[t_1 \left(1 + \frac{x_1}{2} \right) + t_2 \left(1 + \frac{x_2}{2} \right) \right] \frac{3}{2} T \frac{2m^*}{\hbar^2} \left[\rho + \frac{\lambda^3}{2\sqrt{2}\gamma} [1 + (2y - 1)^2] \left(\frac{\rho}{2} \right)^2 \right] \\
& - \frac{1}{4} \left[t_1 \left(\frac{1}{2} + x_1 \right) - t_2 \left(\frac{1}{2} + x_2 \right) \right] \frac{3}{2} T \frac{2m^*}{\hbar^2} \left[\left(\frac{\rho}{2} \pm (2y - 1) \frac{\rho}{2} \right) + \frac{\lambda^3}{2^{5/2}\gamma} \left(\frac{\rho}{2} \pm (2y - 1) \frac{\rho}{2} \right)^2 \right] \\
& + \frac{3}{4} t_0 \rho \mp \left(\frac{1}{2} + x_0 \right) t_0 (2y - 1) \left(\frac{\rho}{2} \right) \\
& + \frac{(\alpha + 2)}{16} t_3 \rho^{\alpha+1} - \frac{1}{6} \left(\frac{1}{2} + x_3 \right) t_3 \left[\alpha (2y - 1)^2 \left(\frac{\rho}{2} \right)^2 \pm (2y - 1) \left(\frac{\rho}{2} \right) \rho \right] \rho^{\alpha-1}
\end{aligned}$$

$$\begin{aligned}
& + \frac{1}{4}C[\beta + 2(1 \pm 1)]\rho^{\beta+1} + C\left[(\beta + 1 \pm 1)(2y - 1)\left(\frac{\rho}{2}\right) + \beta(2y - 1)^2\left(\frac{\rho}{2}\right)^2\right]\rho^{\beta-1} \\
& + \eta C_s \rho^{\eta-1},
\end{aligned} \tag{58}$$

$$\begin{aligned}
P(\rho, y, T) = & \left(\frac{5}{2} - \frac{3m^*}{2m}\right)T\rho + \left(\frac{5}{2} - \frac{3m^*}{2m}\right)\frac{T}{2\sqrt{2}}\left(\frac{\lambda^3}{\gamma}\right)\left(\frac{\rho}{2}\right)^2 \\
& + \frac{3}{8}t_0\rho^2 + \frac{(\alpha+1)}{16}t_3\rho^{\alpha+2} + \frac{(\beta+1)}{4}C\rho^{\beta+2} + (\eta-1)C_s\rho^\eta \\
- & \left[t_0\left(\frac{1}{2} + x_0\right) + \left(\frac{\alpha+1}{6}\right)t_3\left(\frac{1}{2} + x_3\right)\rho^\alpha - \left(\frac{5}{2} - \frac{3m^*}{2m}\right)\frac{T}{2\sqrt{2}}\left(\frac{\lambda^3}{\gamma}\right) - (\beta+1)C\rho^\beta\right](2y-1)^2\left(\frac{\rho}{2}\right)^2 \\
& + (\beta+1)C\rho^{\beta+1}(2y-1)\left(\frac{\rho}{2}\right),
\end{aligned} \tag{59}$$

$$\begin{aligned}
\mathcal{E}(\rho, y, T) = & \frac{3}{2}T\rho + \frac{3}{8}t_0\rho^2 + \frac{1}{16}t_3\rho^{\alpha+2} + \frac{3}{2}\frac{T}{2\sqrt{2}}\left(\frac{\lambda^3}{\gamma}\right)\left(\frac{\rho}{2}\right)^2 + \frac{1}{4}C\rho^{\beta+2} + C_s\rho^\eta \\
- & \left[t_0\left(\frac{1}{2} + x_0\right) + \left(\frac{1}{6}\right)t_3\left(\frac{1}{2} + x_3\right)\rho^\alpha - \frac{3}{2}\frac{kT}{2\sqrt{2}}\left(\frac{\lambda^3}{\gamma}\right) - C\rho^\beta\right](2y-1)^2\left(\frac{\rho}{2}\right)^2 \\
& + C\rho^{\beta+1}(2y-1)\left(\frac{\rho}{2}\right),
\end{aligned} \tag{60}$$

$$\begin{aligned}
TS(\rho, y, T) = & T\rho\left[\frac{5}{2} - y\ln\left(\frac{\lambda^3}{\gamma}y\rho\right) - (1-y)\ln\left(\frac{\lambda^3}{\gamma}(1-y)\rho\right)\right] \\
& + \frac{T}{2\sqrt{2}}\left(\frac{\lambda^3}{\gamma}\right)\frac{[1+(2y-1)^2]}{2}\left(\frac{\rho}{2}\right)^2
\end{aligned} \tag{61}$$

Here, for the proton density (ρ_p) and neutron density (ρ_n), we defined, the isoscalar density ρ , isovector density ρ_3 , proton fraction y and related quantities by

$$\begin{aligned}
\rho & = \rho_p + \rho_n, & \rho_3 & = \rho_p - \rho_n = (2y-1)\rho, & y & = \rho_p/\rho, \\
\rho_p & = \frac{1}{2}(\rho + \rho_3) = y\rho, & \rho_n & = \frac{1}{2}(\rho - \rho_3) = (1-y)\rho, \\
\sum_q \rho_q^2 & = \frac{1}{2}(\rho^2 + \rho_3^2) = \frac{[1+(2y-1)^2]}{2}\rho^2 = [1+2y(y-1)]\rho^2, \\
\sum_q \rho_q^3 & = \frac{1}{4}\rho(\rho^2 + 3\rho_3^2) = \frac{[1+3(2y-1)^2]}{4}\rho^3 = [1+3y(y-1)]\rho^3
\end{aligned} \tag{62}$$

The \pm in μ_q stands + for q =proton and - for neutron.

At fixed T and P , only one of either ρ or y is the independent variable. Thus observables such as P , \mathcal{E}/ρ , \mathcal{S}/ρ may have a discontinuity in T or y when $\left(\frac{\partial\rho}{\partial T}\right)_{y,P}$ or $\left(\frac{\partial\rho}{\partial y}\right)_{T,P}$ diverges. We can study the behavior of thermodynamic quantities at a fixed P using $dP = 0$ from Eq.(59),

$$\begin{aligned}
dP = & \left\{ \left(\frac{5}{2} - \frac{3m^*}{2m}\right)\left[\rho - \frac{1}{2}\frac{1}{2\sqrt{2}}\left(\frac{\lambda^3}{\gamma}\right)\left(\frac{\rho}{2}\right)^2 - \frac{1}{2}\frac{1}{2\sqrt{2}}\left(\frac{\lambda^3}{\gamma}\right)(2y-1)^2\left(\frac{\rho}{2}\right)^2\right] \right\} dT \\
& + \left\{ \left[\frac{5}{2} - \frac{3}{2}\left(\frac{m^*}{m}\right)^2\right]T + \frac{3}{4}t_0\rho + \frac{(\alpha+2)(\alpha+1)}{16}t_3\rho^{\alpha+1} \right. \\
& + \left[\frac{35}{8} - \frac{15m^*}{4m} + \frac{3}{8}\left(\frac{m^*}{m}\right)^2\right]\frac{T}{2\sqrt{2}}\left(\frac{\lambda^3}{\gamma}\right)\left(\frac{\rho}{2}\right) + \frac{(\beta+2)(\beta+1)}{4}C\rho^{\beta+1} + \eta(\eta-1)C_s\rho^{\eta-1} \\
& - \left[t_0\left(\frac{1}{2} + x_0\right) + \left(\frac{\alpha+2}{2}\right)\left(\frac{\alpha+1}{6}\right)t_3\left(\frac{1}{2} + x_3\right)\rho^\alpha - \left(\frac{\beta+2}{2}\right)(\beta+1)C\rho^\beta \right. \\
& - \left.\left.\left(\frac{35}{8} - \frac{15m^*}{4m} + \frac{3}{8}\left(\frac{m^*}{m}\right)^2\right)\frac{T}{2\sqrt{2}}\left(\frac{\lambda^3}{\gamma}\right)\right](2y-1)^2\left(\frac{\rho}{2}\right) \right. \\
& \left. + (\beta+2)(\beta+1)C\rho^\beta(2y-1)\left(\frac{\rho}{2}\right) \right\} d\rho \\
- & \left\{ \left[t_0\left(\frac{1}{2} + x_0\right) + \left(\frac{\alpha+1}{6}\right)t_3\left(\frac{1}{2} + x_3\right)\rho^\alpha - (\beta+1)C\rho^\beta \right. \right. \\
& \left. \left. - \left(\frac{5}{2} - \frac{3m^*}{2m}\right)\frac{T}{2\sqrt{2}}\left(\frac{\lambda^3}{\gamma}\right)\right](2y-1)\left(\frac{\rho}{2}\right)^2 - (\beta+1)C\rho^\beta\left(\frac{\rho}{2}\right)^2 \right\} 4dy
\end{aligned} \tag{63}$$

This equation gives $y_E(\rho)$ where both $\partial P/\partial y = 0$ and $\partial \rho/\partial y = 0$,

$$y_E(\rho) = \frac{1}{2} + \frac{1}{2} \frac{(\beta + 1)C\rho^\beta}{\left[t_0 \left(\frac{1}{2} + x_0 \right) + \left(\frac{\alpha+1}{6} \right) t_3 \left(\frac{1}{2} + x_3 \right) \rho^\alpha - (\beta + 1)C\rho^\beta - \left(\frac{5}{2} - \frac{3}{2} \frac{m^*}{m} \right) \frac{T}{2\sqrt{2}} \left(\frac{\lambda^3}{\gamma} \right) \right]}. \quad (64)$$

The $y_E(\rho)$ is independent of ρ for momentum independent Skyrme interaction with $x_3 = -1/2$ and $\beta = 0$ as considered in Ref.[10, 11]. The x_3 term and the density dependent effective mass for a momentum dependent Skyrme force introduce a small ρ -dependence in y_E . Eq.(59) shows that, for ρ -dependent y_E , the $P(\rho)$ curve for different values of y at fixed T may cross at some ρ . Moreover, the minimum pressure for a given T and ρ (i.e., $(\partial P/\partial y)_{\rho,T} = 0$) occurs at $y = y_E(\rho) \neq 0.5$ due to Coulomb effect. These results were not seen in Ref.[9]. At y_E , the pressure of the coexistence curve is minimum and the liquid and gas phases have the same proton fraction y_E . The condition $\partial P/\partial y = 0$ determines the equal fraction point y_E .

III. APPLICATIONS TO NUCLEAR MECHANICAL AND CHEMICAL INSTABILITY AND THE LIQUID-GAS PHASE TRANSITION

A. Mechanical and Chemical Instability

We now use the results to discuss features of the instability of nuclei, both mechanical and chemical, and the liquid-gas phase transition. The region of mechanical instability is determined by the condition

$$\left. \frac{dP}{d\rho} \right|_{y,T} = 0 \quad (65)$$

Fig.1 shows the behavior of the pressure $P(\rho, y, T)$ as a function of ρ for several values of the proton fraction y . All curves are at $T = 10$ MeV. The range of y is from $y = 0$, or pure neutron matter, to $y = 1$, or pure proton systems. The point $y = 1/2$ corresponds to symmetric systems. Without a Coulomb interaction results would be symmetric about the point $y = 1/2$ which would also be the point of equal concentration in a liquid/gas phase coexistence. Including a Coulomb interaction shift the equal concentration point to a proton fraction of $y = y_E(\rho) \sim 0.415$ with a momentum dependence included in the interaction and to $y = y_E = 0.41057$ without a momentum dependence. The $y = y_E$ curve for both the momentum dependent and independent cases has the lowest pressure versus density dependence, i.e., the lowest P for a given value of ρ at a given T . A higher or lower y raises the pressure at a given density. Both a momentum dependent Skyrme interaction and a momentum independent Skyrme interaction results are shown for several values of y and they are distinguished by the thickness of the lines as described in the figure caption. The momentum dependence increases the pressure in the range shown (thick lines compared to thin lines) and introduces the density dependence of $y_E(\rho)$ given by Eq.(64). The mechanical instability densities for each y curve at $T = 10$ MeV are the points where the $P(\rho, y, T)$ curve has zero slope, $dP/d\rho|_{y,T} = 0$. The total region of mechanical instability is obtained by a similar calculation of $P(\rho, y, T)$ at different T . For a one component system or a symmetric system the mechanical instability region is a curve somewhat similar to an inverted parabola with its peak at the critical point. Allowing for systems with different values of y gives a two dimensional boundary surface for the mechanical instability region. The intersection of the surface with different y planes gives the one dimensional boundary curve or line of mechanical instability for each corresponding value of y .

Fig.2 shows the proton fraction y versus the density ρ for different fixed values of the pressure at a fixed temperature of $T = 10$ MeV. The loops and curves are determined by solving $P(\rho, y, T) = P$ for the values of P listed in the figure caption and at the temperature $T = 10$ MeV. Fig.2 is obtained from Fig.1 by drawing a horizontal line and looking at the points where the horizontal line intersects the set of $P(\rho, y, T)$ curves. This intersection can be at one, two or three points. Besides the inner most closed loop ($P = 0$) shown in Fig.2, a vertical line exists at $\rho = 0$ for $P = 0$ for all $y = 0 \sim 1$. Similarly, for the second inner closed loop at $P = 0.015$ MeV/fm³, a nearly parallel vertical line is present at very low density. The right most point on each curve and the left most point on a closed loop with $d\rho/dy|_{P,T} = 0$ are at the point of equal concentration y_E . Also shown are two thin lines for $y_E(\rho)$. The dashed thin line is at $y_E = 0.41057$ and is horizontal or density independent and corresponds to the momentum independent interaction. The solid thin line is nearly horizontal with a slight density dependence and has $y_E(\rho) = 0.4106 \sim 0.4214$ for $\rho = 0 \sim 0.15$ fm⁻³. Horizontal turning points on each curve occur at $dy/d\rho|_{P,T} = 0$. For each T , there is a curve $P(\rho)|_{y,T}$ with an inflection point for a particular y which we call y_I . At the pressure $P = P(\rho, y_I, T)$, the closed loop in Fig.2 just breaks at the point of $y = y_E$ on the left low density side and creates two new horizontal turning points with $\partial y/\partial \rho = 0$. Fig.2 also shows the result that a momentum independent force has closed loops outside those of

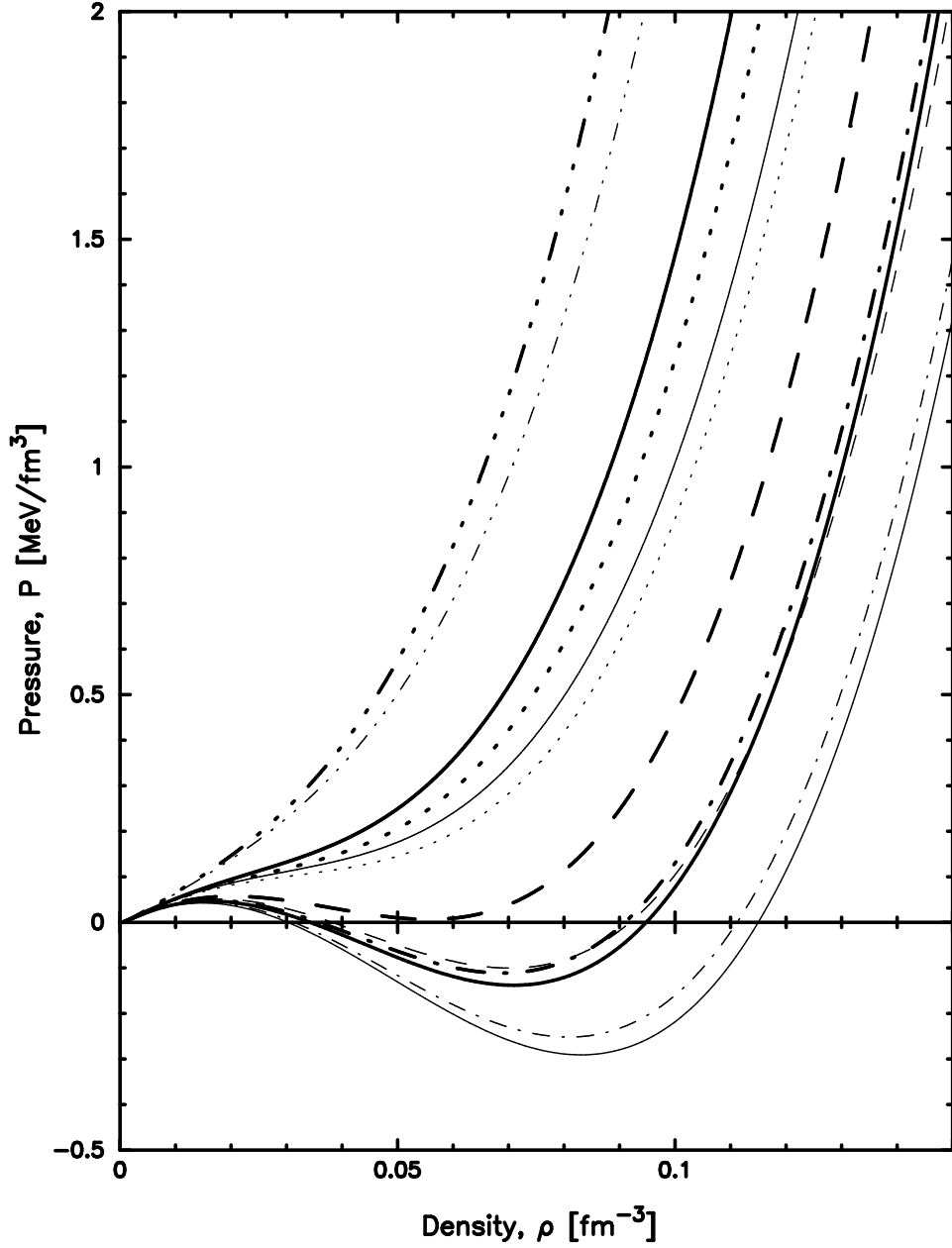


FIG. 1: Pressure $P(\rho)$ versus ρ at $T = 10$ MeV for various proton fraction y . The upper solid curve is for $y = 0$, dashed curve for $y = 0.2$, dash-dotted curve for $y = 0.5$, dotted curve for $y = 0.8$, and dash-dot-dot-dotted curve for $y = 1$. The thick curves are for the momentum dependent Skyrme force and the thin curves are for the momentum independent Skyrme force. The lower thick solid curve is for $y = y_E(\rho)$ of Eq.(64) ($y_E = 0.4106 \sim 0.4214$ for $\rho = 0 \sim 0.15 \text{ fm}^{-3}$) with momentum dependent Skyrme force and the lower thin solid curve is for $y = y_E = 0.41057$ with momentum independent Skyrme force.

a momentum dependent force and open curves to the right of those of a momentum dependent force with the same pressure P .

The region of chemical instability (spinodal in $\mu(y)|_{P,T}$) is determined by the condition

$$\left. \frac{d\mu_q}{dy} \right|_{P,T} = 0 \quad (66)$$

for each component $q = p$ or n . These conditions for either protons or neutrons give the same relation since

$$y d\mu_p + (1 - y) d\mu_n = \frac{1}{\rho} dP \quad (67)$$

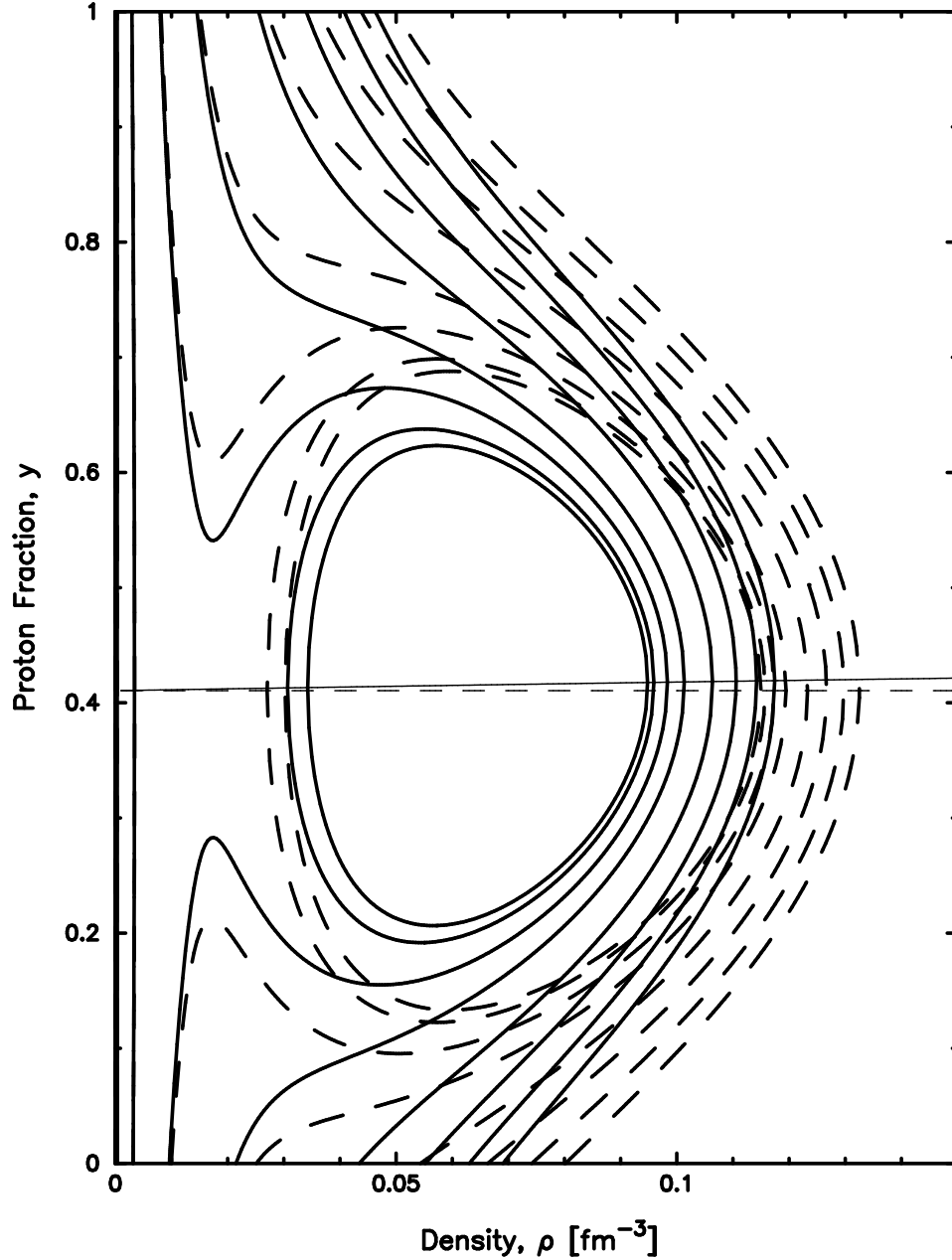


FIG. 2: Proton fraction $y(\rho)$ for $P = 0, 0.015, 0.05, 0.1, 0.2, 0.3, 0.4,$ and $0.5 \text{ MeV}/\text{fm}^3$ from inside to outside at $T = 10 \text{ MeV}$. The solid curves are for the momentum dependent Skyrme force and the dashed curves are for the momentum independent Skyrme force. The thin straight lines are $y_E(\rho)$ for the corresponding force.

This general condition will be used later in our discussion of results given in various figures. The result is also useful for checking numerical results. The chemical instability condition can be rewritten in terms of derivatives of the chemical potential and pressure with respect to the density variable ρ and proton fraction y . Namely, the chemical instability condition can be obtained from the following relation [11]

$$\left. \frac{dP}{d\rho} \right|_{y,T} \left. \frac{d\mu_q}{dy} \right|_{\rho,T} = \left. \frac{dP}{dy} \right|_{\rho,T} \left. \frac{d\mu_q}{d\rho} \right|_{y,T} \quad (68)$$

The expressions developed for the proton and neutron chemical potentials are functions of the variables (ρ, y, T) . The equation of state $P(\rho, y, T)$ can then be used to find their behaviors in terms of (y, P, T) or (ρ, P, T) . The behaviors with y of the proton chemical potential $\mu_p(\rho, P, T) \rightarrow \mu_p(y)$ and neutron chemical potential $\mu_n(\rho, P, T) \rightarrow \mu_n(y)$ at various values of the pressure P and at a fixed temperature $T = 10 \text{ MeV}$ are shown in Fig.3. The chemical instability

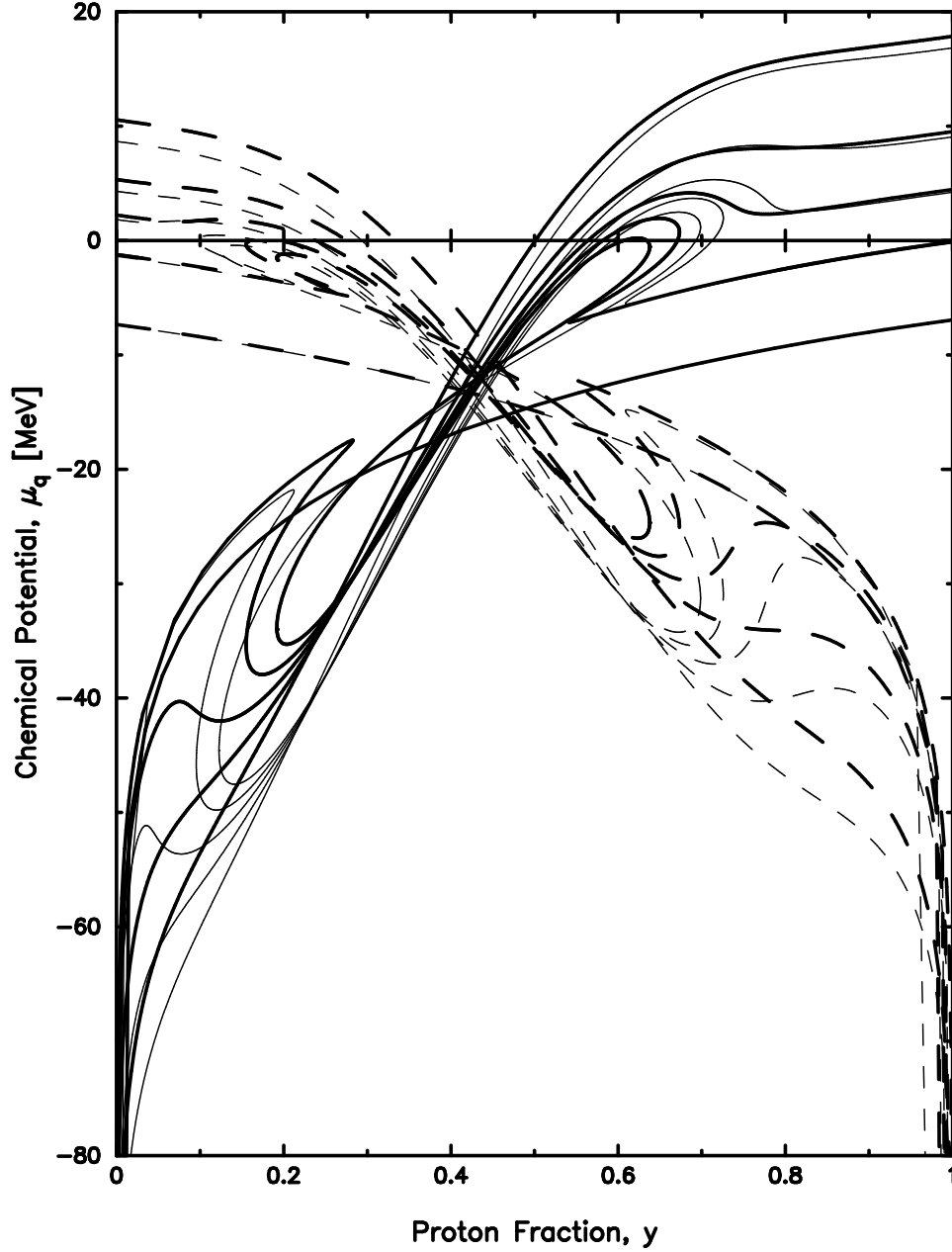


FIG. 3: Chemical potential $\mu_p(y)$ and $\mu_n(y)$ for $P = 0.015, 0.05, 0.1, 0.2,$ and 0.5 from top to bottom curve for protons (solid curve) and from bottom to top curve for neutrons (dashed curve) at $T = 10$ MeV. Thick curves are for momentum dependent Skyrme force and the thin curves for momentum independent Skyrme force.

region boundaries are determined by the points where the slope of each chemical potential with respect to y is zero. Further discussion of the chemical spinodal line is given in the next subsection. The behaviors of the proton chemical potential $\mu_p(\rho, P, T) \rightarrow \mu_p(\rho)$ and neutron chemical potential $\mu_n(\rho, P, T) \rightarrow \mu_n(\rho)$ with density ρ at various fixed values of the pressure P and at a fixed temperature $T = 10$ MeV are shown in Fig.4. Fig.2 and Fig.4 show some similarities in the behavior of the plotted quantities, i.e., inner closed loops at low pressure, to outer curves that almost form closed loops with increasing pressure, to open curves with further increases in pressures.

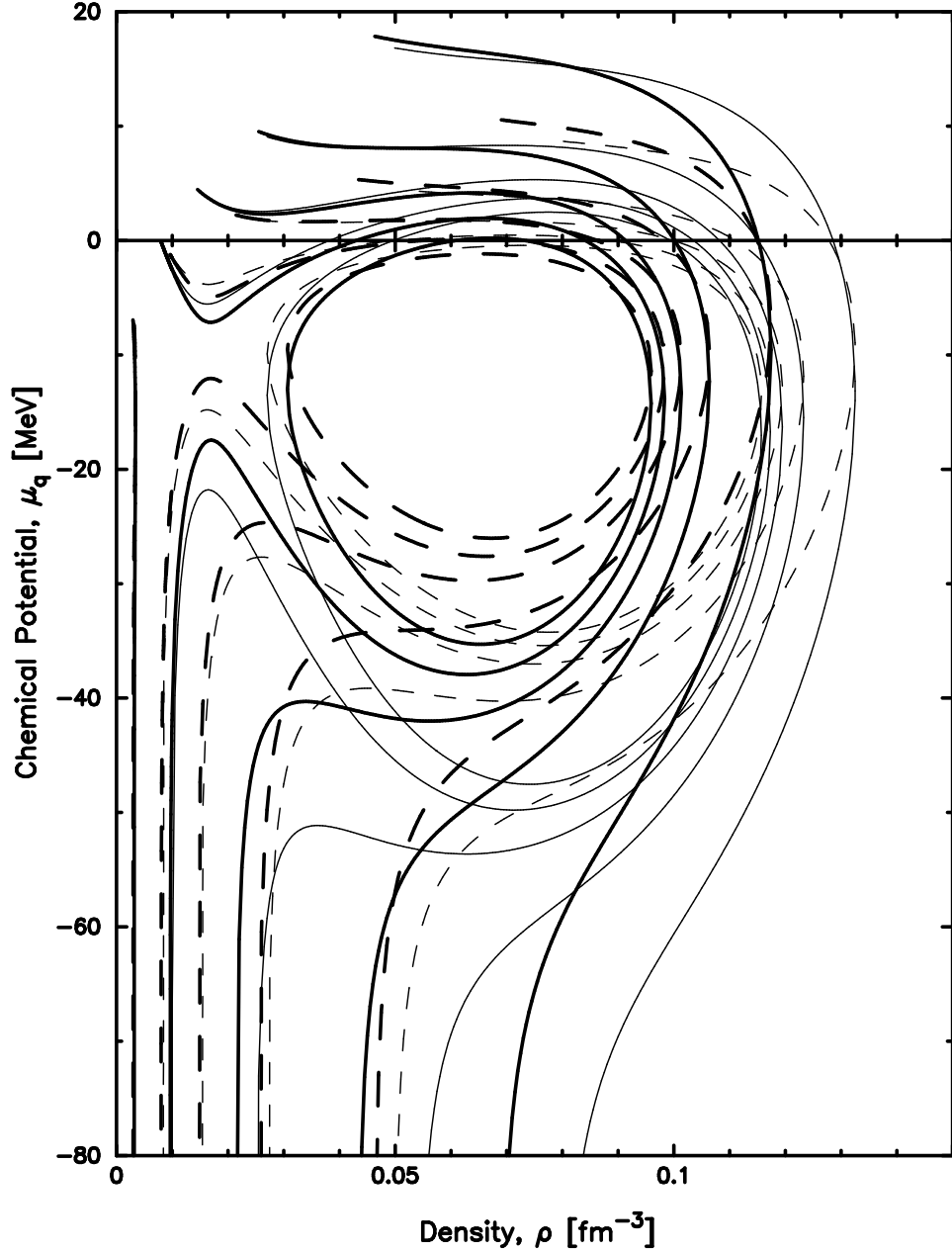


FIG. 4: Same as Fig.3 but for $\mu_p(\rho)$ and $\mu_n(\rho)$ versus ρ .

B. Liquid-Gas Phase Transition and the Coexistence Curve

For a one component system the coexistence curve is a line obtained by the familiar Maxwell construction as already noted. For a two component system the coexistence region is a surface obtained as follows. The condition for coexistence between the two phases requires the proton chemical potentials to be the same in two phases and, similarly, the neutron chemical potentials must be the same in the two phases at a given pressure and temperature. Note that the proton fraction need not be the same in each of the two phases. In fact, the liquid phase should be a more symmetric system than the gas phase because of the symmetry potential as seen in Refs.[10, 11]. Figs.5-9 show features of the coexistence curves together with the mechanical and chemical instability curves.

The condition of phase coexistence corresponds to a rectangular box geometrical construction in the chemical potential plots of Fig.3 or of Fig.4. Namely, the chemical potential equality condition $\mu_p(y_1, P, T) = \mu_p(y_2, P, T)$ and $\mu_n(y_1, P, T) = \mu_n(y_2, P, T)$ leads to a rectangular box in Fig.3 with vertical sides connecting the $\mu_p(y_1, P, T)$ to the $\mu_n(y_1, P, T)$ for side 1 and the $\mu_p(y_2, P, T)$ to the $\mu_n(y_2, P, T)$ for side 2. The horizontal sides are the chemical

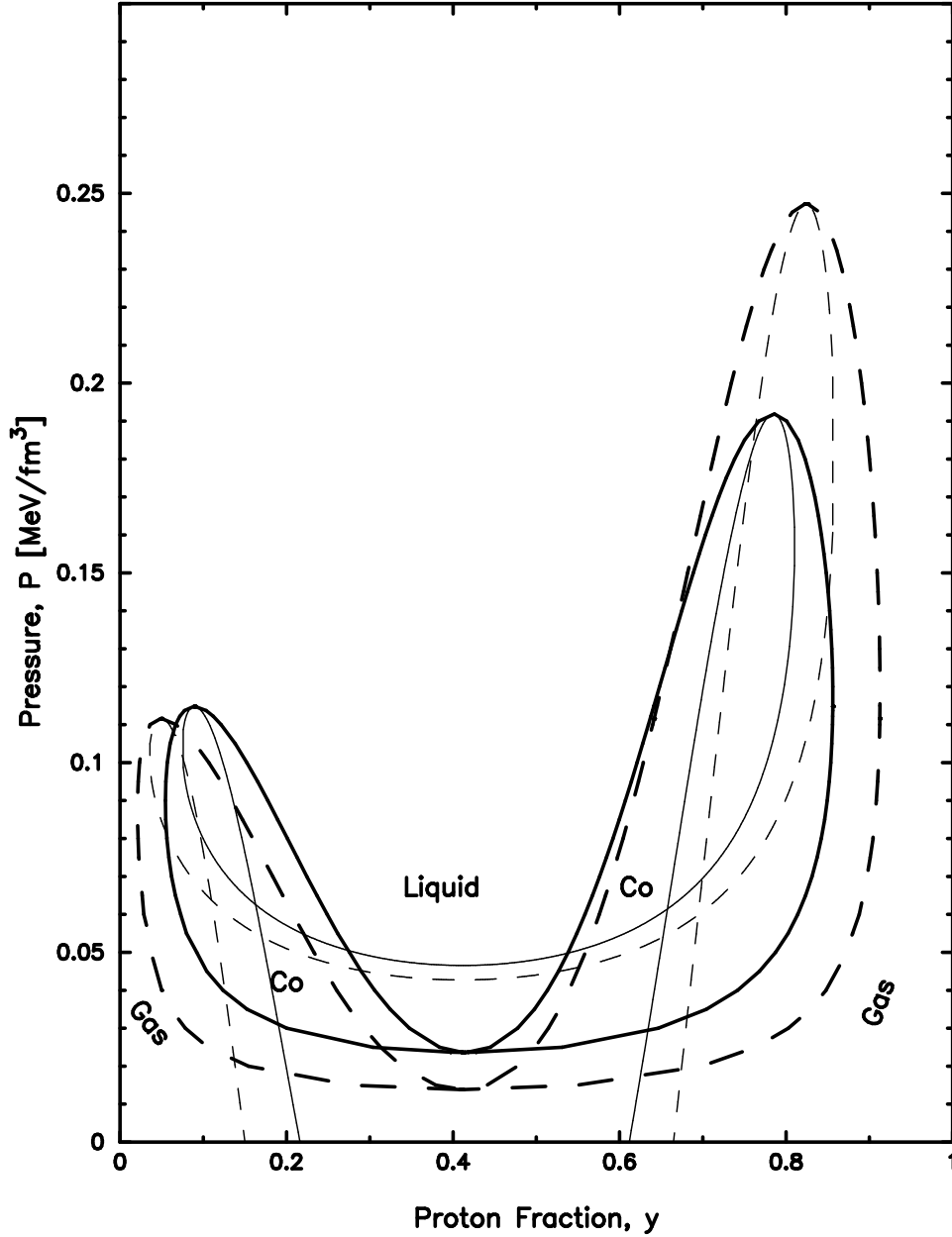


FIG. 5: Pressure P versus proton fraction y for coexistence loop (thick curves) at $T = 10$ MeV. The solid curve is for the momentum dependent Skyrme force and the dashed curve is for momentum independent Skyrme force. The thin curves are the chemical instability boundary curves for each case of Skyrme interaction respectively. For both momentum dependent and momentum independent cases the maximum of the chemical instability loop and the coexistence loop occur at the same point where the curves are tangent to each other as discussed in the text. The point of equal concentration is $y_E \sim 0.415$ for momentum dependent case and $y_E = 0.41057$ for momentum independent case.

potential equality conditions at y_1 and y_2 for neutrons and for protons. The rectangular box shrinks in its horizontal direction in μ_q - y plots as the point of equal concentration, where the liquid and gas phases have the same proton fraction, is approached (the lowest point of the coexistence curve in Fig.5).

Fig.5 shows various features of the coexistence region in pressure versus proton fraction. The coexistence region are the dark thicker solid line for a momentum dependent force and the dark thicker dashed line for a momentum independent force. Also shown are associated chemical instability regions as a thinner solid line, and thinner dashed line. The calculations are done at a temperature of 10 MeV. For a two component system, the coexistence and instability regions are two dimensional surfaces in pressure, temperature and proton fraction as mentioned above. The pressure-proton fraction behavior shown is a consequence of cutting these surfaces with a constant temperature

plane. The result at $T = 10$ MeV are the loops shown. Other temperatures can be obtained in a similar fashion. For a momentum independent force the chemical instability region basically lies inside the coexistence curve and peaks at the top of the coexistence loop, the critical points. The condition $dP/dy|_T = 0$ with $d^2P/dy^2|_T < 0$ gives a critical point on the coexistence curve and the condition $dy/dP|_T = 0$ gives the point with maximal asymmetry at the left and right most points of coexistence curve. The proton rich $y \geq y_E$ and neutron rich $y \leq y_E$ loops are very asymmetric because of the Coulomb interaction. The inclusion of velocity or momentum dependent interactions leads to further modification of the coexistence curve and chemical instability curves. This modification is easily seen in the figure by comparing the dashed momentum independent curves with the solid momentum dependent case. The figure shows that the momentum dependent interaction that was used has a larger effect on the asymmetric proton rich loop ($y > y_E$) significantly reducing its maximum pressure. The maximum of the neutron rich loop ($y < y_E$) remains somewhat unchanged with a small increase. Another effect is to shift the two loops inward toward the equal concentration point y_E . A third effect is to shift the lowest pressure point, which occurs at the equal concentration y_E , upward with the value of y_E nearly unchanged. Finally, it should be noted that the peaks of the coexistence and chemical instability curves are at the same point where the curves are tangent to each other. We see no indication of a truncation effect in our model where the coexistence curve intersects the chemical instability curve before reaching the peak critical point. A truncation effect gives a limiting pressure (below the maximum pressure of the chemical instability curve) above which a liquid-gas phase transition cannot take place [22].

Fig.6 shows plots in y versus ρ of phase coexistence curves, instability boundary loops for both chemical and mechanical instability, and features of $\partial\mu_q/\partial\rho|_{y,T} = 0$ for proton and neutrons. The thin curves are for a momentum independent interaction and the thick curves are for a momentum dependent interaction. The calculations are done at a fixed temperature of 10 MeV. Some features common to both cases are as follows. The mechanical and chemical instability boundary curves are closed loops with the mechanical loop (dashed line) inside the chemical instability loop (solid line). These two loops touch at y_E , the dash-dot-dot-dotted line. The $y_E(\rho)$ increases slightly with ρ for a momentum dependent interaction while it is constant (horizontal) for a momentum independent interaction. The ρ dependence of $y_E(\rho)$ come from the ρ dependence of the effective mass and also from the x_3 term as can be seen in Eq.(64). Also intersecting at these same points are $\partial\mu_p/\partial\rho = 0$ and $\partial\mu_n/\partial\rho = 0$. Different features and behaviors exist between the two cases. The momentum dependent case (thick curves) has behaviors that are compressed in these y - ρ plots. The coexistence curves have a different quantitative but similar qualitative behavior between the two cases. The coexistence loop (dash-dotted line) is outside the other two loops and tangent to chemical instability loop at two points. These two points are the critical points of low and high y which are shown in Fig.5 where the two loops touch at the peak of each loop. Comparing the two cases quantitatively, we see a compression of the results of the momentum dependent case (thick curves) with respect to the results of the momentum independent case (thin curves). The thick loops are inside of thin loops.

Fig.7 and Fig.8 show chemical potentials for both proton μ_p and neutron μ_n and pressure P along the various curves of coexistence and chemical and mechanical instabilities. Curves in Fig.7 illustrate the behavior of each chemical potential with density on the left panel and proton fraction on the right panel. Curves in Fig.8 are pressure versus density on the left side and pressure versus proton fraction on the right. The separate pressure-proton fraction behaviors in Fig.8 were already shown in Fig.5, but now these two figures contain additional plotted quantities which are the $\partial\mu_q/\partial\rho|_{y,T} = 0$ curves. The chemical potential density curves in Fig.7 have features similar to those discussed in Fig.6. Both momentum dependent and independent cases of Fig.7 and Fig.8 shows tangent points of the solid line and dash-dotted line. Also seen in these figures are the compression or shrinking of various curves for momentum dependent case with respect to the momentum independent case. The thick loops are inside of thin loops. Fig.5 shows that the momentum dependent interaction leaves the point of equal concentration nearly unchanged i.e., from $y = 0.4106$ to $y \approx 0.415$.

Fig.9 shows the behavior of the boundary curves of the proton and neutron chemical potentials with pressure for both momentum dependent and momentum independent Skyrme interactions. A comparison of the thick curves (momentum dependent case) and thin curves (momentum independent case) shows that the qualitative behavior is the same. Quantitative difference exist with the momentum independent behavior being an enlargement of the momentum dependent shape. The coexistence arc and the chemical instability loop meet at the cusp. The behavior shown in these figures also confirm that no truncation effects exist in our study.

IV. SUMMARY AND CONCLUSIONS

In this paper we studied the thermodynamic properties of a two component system of hadronic matter made of protons and neutrons. Our analysis is based on a mean field model using a local Skyrme interaction and includes both velocity or momentum dependent and momentum independent interactions, besides volume, symmetry and Coulomb effects. We have used a somewhat simplified description of the velocity dependence of the nuclear interaction.

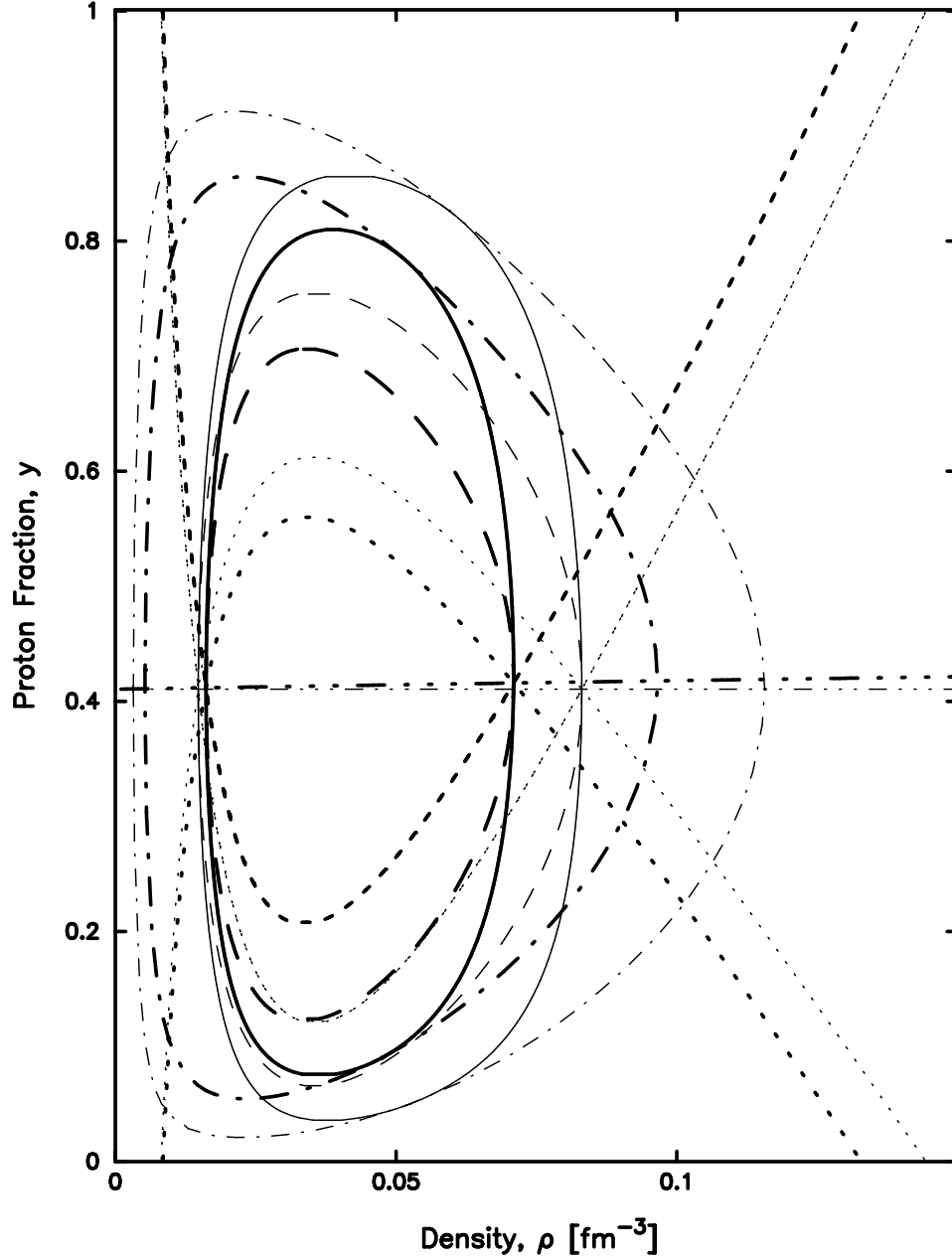


FIG. 6: Figure shows the coexistence curves (dash-dotted line), chemical instability boundary curves (solid line) and mechanical instability boundary curves (dashed line) at $T = 10$ MeV. Also shown are the $\partial\mu_q/\partial\rho = 0$ curves for proton (dotted line) and for neutron (short dash line) at $T = 10$ MeV. The dash-dot-dot-dotted line is for $y_E(\rho)$. The thick lines are for momentum dependent Skyrme force and the thin lines are for momentum independent Skyrme force. The momentum dependent loops are inside the momentum independent loops.

In particular we have used a density dependent effective mass approximation. Effective mass approximations are frequently used in physics to capture the main effects and they lead to a simpler set of equations and a corresponding simpler analysis. As noted we still keep Coulomb and surface terms which are present in realistic nuclear systems. It is the interplay of volume, surface, symmetry and Coulomb and momentum dependent terms that is studied here. In fact, the interplay of such terms makes nuclei a unique system for studying phase transitions, chemical and mechanical instability in binary systems. We then applied the basic thermodynamic relations that we developed to issues related to the mechanical and chemical instability of nuclei and features associated with a liquid/gas phase transition in this system.

Because of the two component nature of real nuclear systems, the analysis involves a study of the behavior in proton

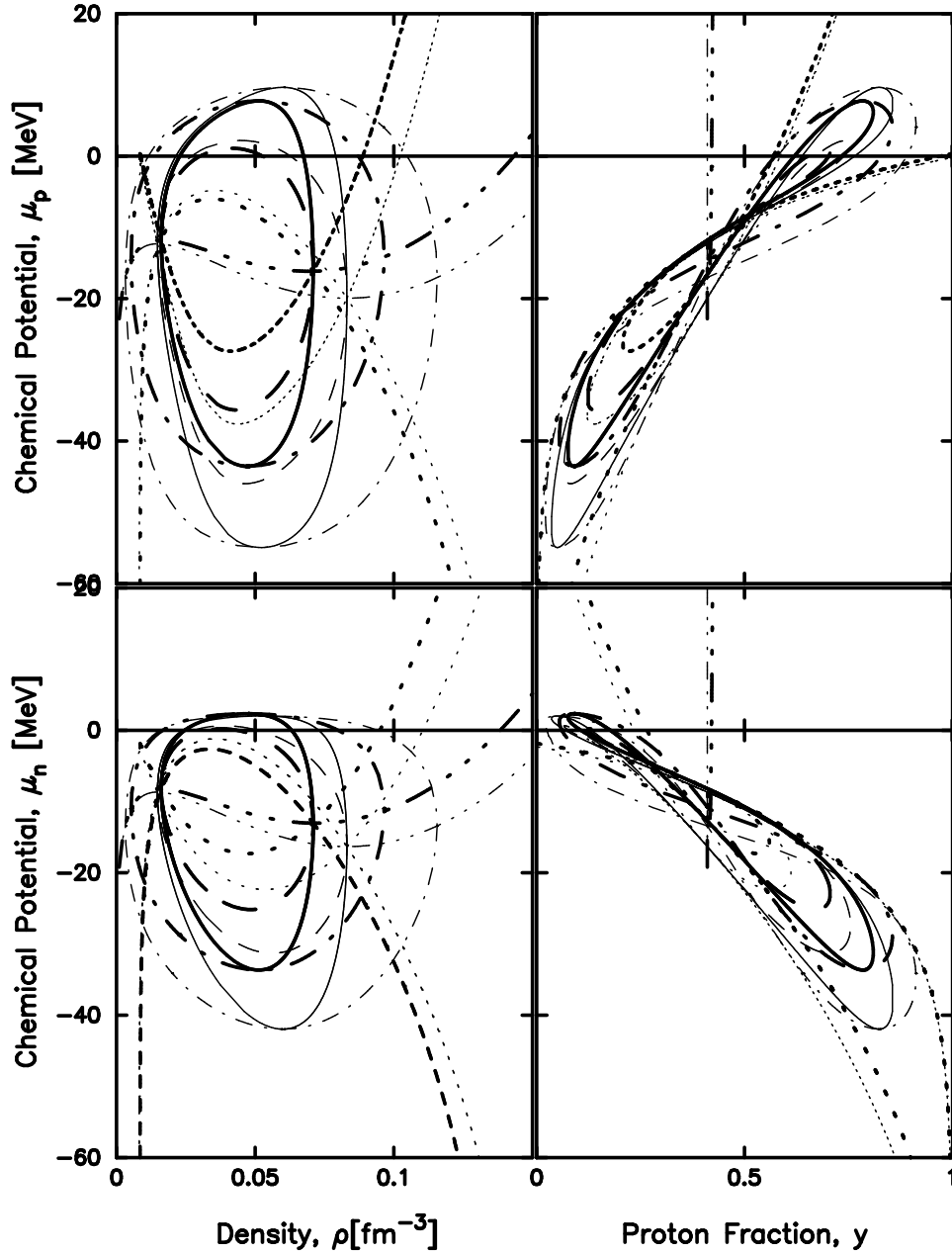


FIG. 7: Chemical potential μ_p (upper panel) and μ_n (lower panel) for various boundary curves at $T = 10$ MeV. The curves are same as in Fig.6.

fraction, density and temperature (y, ρ, T) and also proton fraction, pressure and temperature (y, P, T) . We studied systems with proton fraction $y = 0 \sim 1$, where $y = 0$ corresponds to a system of pure neutrons and $y = 1$ is for a system of pure protons. An important system with large neutron excess is a neutron star. The study of nuclear systems with arbitrary proton/neutron ratios is also important for future RIB experiments and for medium energy collisions where the liquid/gas phase transition is studied experimentally. In a liquid/gas phase transition the liquid and gas phase have different proton fractions because of symmetry and Coulomb effects. The proton fraction in the liquid phase reflects a more symmetric system than the gas phase where a higher asymmetry exists. The process of producing a larger neutron excess in the gas phase is referred to as isospin fractionation and a review can be found in Ref.[1, 2, 4, 5, 6, 7]. The process is modified somewhat by the Coulomb interaction which leads to proton diffusion of some protons from the liquid phase back into the gas phase as discussed in Ref.[10, 11].

One of the unique aspects of the nuclear systems is a velocity or momentum dependence in the two body interaction. Here, we also study the role of this momentum dependence first in the thermodynamic properties of the system. Then,

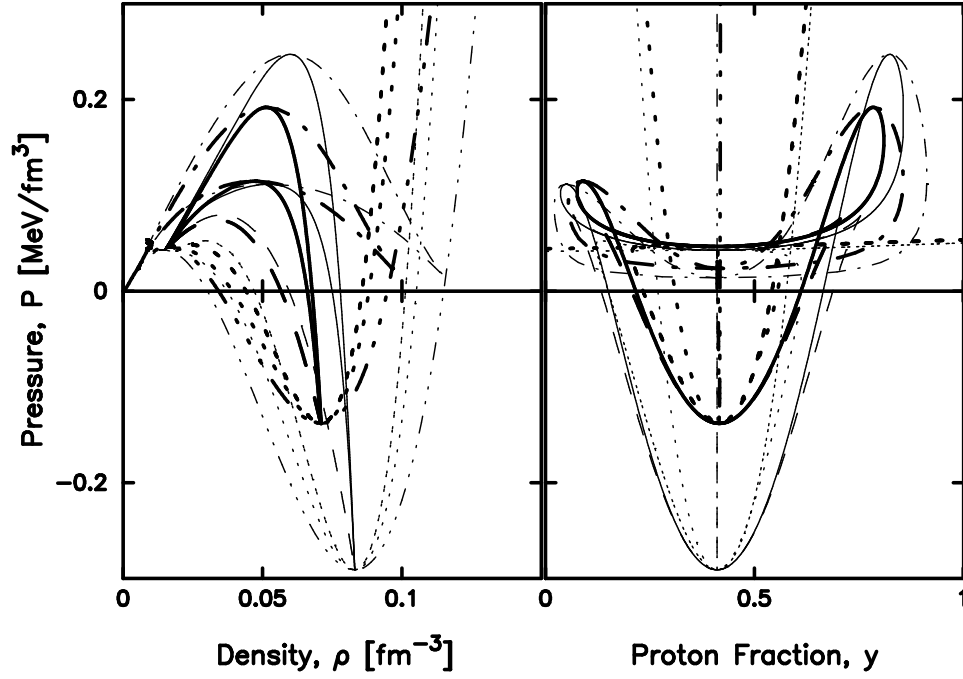


FIG. 8: Pressure P for various curves. The curves are same as in Fig.6.

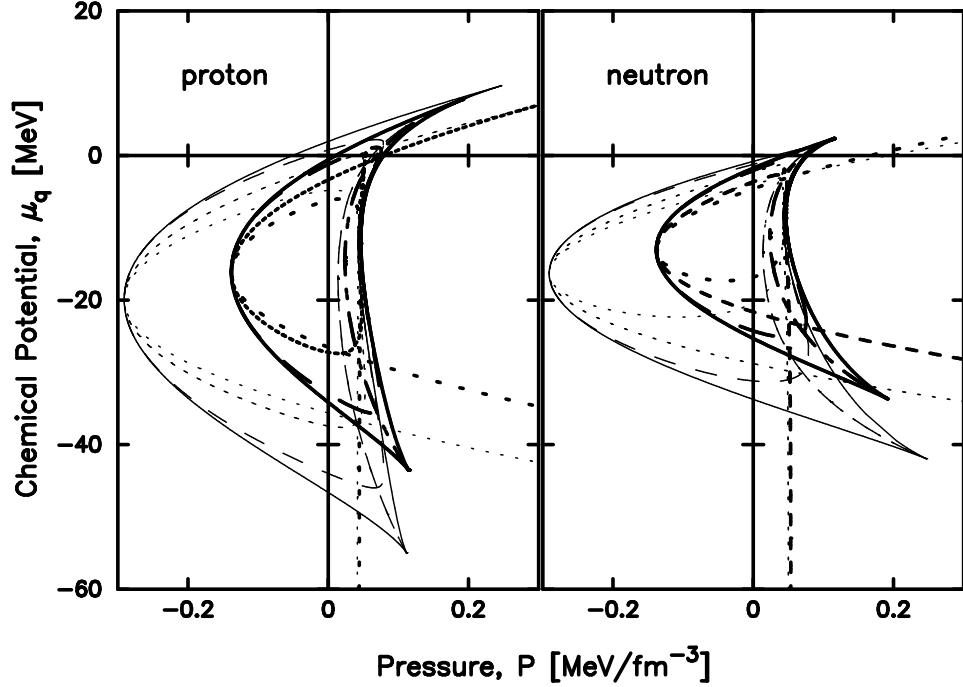


FIG. 9: Chemical potential μ_q versus pressure P for various boundary curves. The left panel is for proton μ_p and the right panel is for neutron μ_n . The curves are same as in Fig.6.

we extend the discussion of its role to nuclear instabilities and phase transitions and make a comparison with the case without momentum dependence. A characteristic pattern of qualitative similarities and quantitative differences appear between a momentum or velocity dependent Skyrme interaction and a momentum or velocity independent Skyrme interaction. These patterns can be seen in Fig.1-9 and are discussed in detail in Sect.III which we briefly summarize now.

Fig.1 shows that the momentum dependence increases the pressure at a given density. Fig.2 and Fig.4 show proton

fraction versus density and chemical potential versus density at several pressures and at a fixed temperature. The qualitative features are the same between momentum dependent and momentum independent forces. However, sizeable quantitative differences are present between the two types of interactions. For example the solid loops (momentum dependent interaction) in proton fraction versus density of Fig.2 are reduced versions of the same dashed loops (momentum independent interaction). Similarly, the chemical instability boundaries for a momentum dependent Skyrme interaction are found to be reduced versions of the same boundaries for momentum independent Skyrme interactions as can be seen from Fig.5 and a comparison of the thin curves of Fig.6–9 with the corresponding thick curves of these figures. Fig.5 also shows that momentum dependent terms reduce the height of the proton rich asymmetric loop ($y > y_E$) and leave the height of the neutron asymmetric loop ($y < y_E$) almost unchanged while the lowest pressure point, which is the point of equal concentration y_E , is shifted upward with the value of y_E nearly unchanged. From Fig.5 we also see that the chemical instability loop lie on top of each other for proton and neutron as required by the general connection of Eq.(67). Also seen is that the chemical instability loop is inside the coexistence loop and tangent to it at the maxima of each loop. The largest and smallest y in the coexistence loops are shifted inward towards the point of equal concentration y_E . Figs.6 and 7 shows that the mechanical instability loop is inside the chemical instability loop and tangent at the equal proton fraction $y_E(\rho)$ without touching it at the peak of them.

Acknowledgments

This work was supported in part by the US Department of Energy under DOE Grant No. DE-FG02-96ER-40987. S.J.L. was on sabbatical leave from Kyung Hee University and spent a sabbatical year at Rutgers University in 2006-2007.

-
- [1] C.B. Das, S. Das Gupta, W.G. Lynch, A.Z. Mekjian, and M.B. Tsang, Phys. Rep. **406**, 1 (2005).
 - [2] S. Das Gupta, A.Z. Mekjian, B. Tsang, Adv. in Nucl. Phys. (J. Negele, E. Vogt, ed.), **26**, 89 (2001).
 - [3] H. Jaqaman, A.Z. Mekjian, and L. Zamick, Phys. Rev. **C27**, 2782 (1983).
 - [4] *Isospin Physics in Heavy-Ion Collisions at Intermediate Energies*, Eds. Bao-An Li and W.Udo Schröder (Nova Science Publications, Inc. New York, 2001).
 - [5] H.S. Xu, etal, Phys. Rev. Lett. **85**, 716 (2000).
 - [6] B.A. Li, Phys. Rev. Lett. **85**, 4221 (2000).
 - [7] B.A. Li, L.W. Chen, H.R. Ma, J. Xu, and G.C. Yong, arXiv:0710.2877v1 [nucl-th].
 - [8] H. Jaqaman, A.Z. Mekjian, and L. Zamick, Phys. Rev. **C29**, 2067 (1984).
 - [9] H. Müller and B.D. Serot, Phys. Rev. **C52**, 2072 (1995).
 - [10] S.J. Lee and A.Z. Mekjian, Phys. Rev. **C63**, 044605 (2001).
 - [11] S.J. Lee and A.Z. Mekjian, Phys. Letts. **B580**, 137 (2004).
 - [12] P. Pawlowski, Phys. Rev. **C65**, 044615 (2002).
 - [13] C.B. Das, S. Das Gupta, and A.Z. Mekjian, Phys. Rev. **C67**, 064607 (2003).
 - [14] J.B. Natowitz et al, Phys. Rev. **C65**, 034618 (2002); Phys. Rev. Lett. **89**, 212701 (2002).
 - [15] P. Wang, B.D. Leinweber, A.W. Thomas, and A.G. Williams, Nucl. Phys. **A748**, 226 (2005).
 - [16] N. Buyukcizmeci, R. Ogul, and A.S. Botvina, Eur. Phys. J. **A25**, 57 (2005).
 - [17] O. Lopez, D. Lacroix, and E. Vient, Phys. Rev. Lett. **95**, 242701 (2005).
 - [18] P. Danielewicz, R. Lacey, and W.G. Lynch, Science **298**, 1592 (2002).
 - [19] D.H.E. Gross, *Microcanonical Thermodynamics - Phase Transitions in "Small" Systems* (World Science, Singapore) (2001).
 - [20] P. Chomaz, M. Colonna, and J. Randrup, Phys. Rep. **389**, 263 (2004).
 - [21] G.F. Bertsch and S. Das Gupta, Phys. Rep. **160**, 189 (1988).
 - [22] J. Xu, L.W. Chen, B.A. Li, and H.R. Ma, Phys. Lett. **B650**, 348 (2007); Phys. Rev. **C77**, 014302 (2008).
 - [23] Ch.C. Moustakidis, Phys. Rev. **C76**, 025805 (2007).
 - [24] L.W. Chen, C.M. Ko, and B.A. Li, Phys. Rev. **C72**, 064309 (2005).
 - [25] B.A. Li, Phys. Rev. **C69**, 064602 (2004).
 - [26] P. Ring and P. Schuck, *The Nuclear Many-Body Problem* (Springer-Verlag, New York, 1980); S.J. Lee, Phys. Rev. **C42**, 610 (1990).
 - [27] K. Huang, *Statistical Mechanics*, (John Wiley & Sons, New York, 1987).